SEISMIC TESTING OF A SCALED ROLLER-COMPACTED-CONCRETE GRAVITY DAM

A THESIS SUBMITTED TO
THE GRADUATE SCHOOL OF NATURAL AND APPLIED SCIENCES
OF
MIDDLE EAST TECHNICAL UNIVERSITY

BY

ALI GHARIBDOUST

IN PARTIAL FULFILLMENT OF THE REQUIREMENTS
FOR
THE DEGREE OF MASTER OF SCIENCE
IN
CIVIL ENGINEERING

AUGUST 2016

Approval of the thesis:

SESIMIC TESTING OF A SCALED ROLLER-COMPACTED-CONCRETE GRAVITY DAM

Submitted by **Ali Gharibdoust** in partial fulfillment of the requirements for the degree of **Master of Science in Civil Engineering Department, Middle East Technical University** to,

Prof. Dr. Gülbin Dural Ünver _____
Director, **Graduate School of Natural and Applied Sciences**

Prof. Dr. İsmail Özgür Yaman _____
Head of Department, **Civil Engineering**

Prof. Dr. Barış Binici _____
Supervisor, **Civil Engineering Dept., METU**

Examining Committee Members:

Prof. Dr. Erdem Canbay _____
Civil Engineering Dept., METU

Prof. Dr. Barış Binici _____
Civil Engineering Dept., METU

Assoc. Prof. Dr. Yalın Arıcı _____
Civil Engineering Dept., METU

Assoc. Prof. Dr. Özgür Kurç _____
Civil Engineering Dept., METU

Assoc. Prof. Dr. Ramazan Özçelik _____
Civil Engineering Dept., Akdeniz Uni.

Date: 23.08.2016

I hereby declare that all the information in this document has been obtained and presented in accordance with academic rules and ethical conduct. I also declare that, as required by these rules and conduct, I have fully cited and referenced all material and results that are not original to this work.

Name, Last Name:

Signature:

ABSTRACT

SEISMIC TESTING OF A SCALED ROLLER-COMPACTED-CONCRETE GRAVITY DAM

Gharibdoust, Ali
M.S., Department of Civil Engineering
Supervisor: Prof. Dr. Barış Binici

August 2016, 83 pages

Within the last half-century, seismic response analysis of concrete gravity dams has been extensively studied. Studies reveal that two types of failure modes prevail in the form of dam body cracking or base slide. The literature lacks the conditions that clearly differentiate the two failure types. In this context a state of the art single degree of freedom pseudo-dynamic testing was developed to assess the gravity dam response on smooth foundation interface. Three different hazard levels of earthquake namely, Operational base earthquake (OBE), Maximum design earthquake (MDE) and Maximum characteristic earthquake (MCE) were employed during the course of the study. Subsequently a pushover test was performed to identify the reserve capacity of the scaled dam and its failure mode. The test results demonstrated the tendency of the scaled dam specimen to slide during MCE ground motion and eventually fail due to the rigid body sliding during the pushover test. A comparison was made between tip displacement and base slip acquired from the test and those values obtained from sliding analysis developed by Chopra and Zhang (1991b). Results were found to be in agreement and confirmed the approach by Chopra and Zhang (1991b). Finally the

results were compared with the results from a companion specimen tested by Aldemir et al. (2015), which had a rough dam-foundation interface. It was found that base roughness is detrimental in defining the final failure mode of dams.

Keywords: Pseudo-dynamic testing, concrete gravity dams, base slide, sliding

ÖZ

ÖLÇEKLİ SİLİNDİRLE-SIKIŞTIRILMIŞ-BETON BIR BARAJIN SİSMİK DENEYİ

Gharibdoust, Ali
Yüksek Lisans, İnşaat Mühendisliği Bölümü
Tez Yöneticisi : Prof. Dr. Barış Binici

Ağustos 2016, 83 sayfa

Son yarım asır içerisinde, baraj-zemin-rezervuar etkilerini dikkate alan beton ağırlık barajlar için birçok sismik analiz metodu geliştirilmiştir. Bu çalışmalar iki farklı baraj göçme tipinin var olduğunu göstermiştir: Baraj gövdesindeki çatlaklardan kaynaklı göçme ve taban kayması kaynaklı göçme. Literatürde daha evvel yapılan deneylerde taban pürüzlülüğünün, barajın sismik yükler altındaki davranışına etkisi net bir şekilde belirlenmemiştir. Bu çalışmada, pürüzsüz zemin üzerine inşa edilmiş ölçekli bir barajın üç farklı deprem seviyesine (OBE, MDE ve MCE) maruz kaldığında sismik davranışını belirlemek amacı ile tek dereceli dinamik benzeri deney metodu geliştirilmiştir. Daha sonra bir itme deneyi gerçekleştirilerek, ölçekli barajın nihai kapasitesi ve göçme şekli belirlenmiştir. Pürüzsüz zemine oturan ölçekli baraj numunesi MCE deneyi esnasında kayma göstermiş ve itme deneyinde ise tamamen tabandan kopup kayarak büyük kalıcı deplasmanlar yapmıştır. Ardından Chopra ve Zhang (1991b) tarafından geliştirilen baraj kayma analizi metodu kullanarak elde edilen sonuçlar deney sonuçları ile kıyaslanmıştır. Bu analizden elde edilen sonuçlar

ve deneyden alınan taban kayması ile tepe deplasmanlarının uyum içerisinde olduğu gözlemlenmiştir. Son olarak, bu çalışmanın en önemli hedeflerinden biri olan, taban pürüzlülüğünün baraj deprem sismik davranışı üzerindeki etkisinin belirlenmei için Aldemir v. d. (2015)'in deney sonuçları ile kıyaslamalar yapılmıştır. Sonuçlar, taban pürüzlülük seviyesinin göçme modunu değiştirmekte önemli bir etken olduğunu ortaya koymaktadır.

Anahtar kelimeler: Dinamik Benzeri Deney, Beton Ağırlık Barajlar, Taban Kayması, Kayma

To my dear family …

ACKNOWLEDGEMENTS

I would like to express my deepest gratitude to my supervisor, Prof. Dr. Barış Binici for his guidance, advice, criticism, insight, and encouragement throughout the research.

I would also like to thank Alper Aldemir, for all his guidance, help and support. I appreciate his generosity in sharing his knowledge with no hesitation and his assistance during execution of experiments.

I would like to thank my lovely mom, Nasrin Roumianfar, my dad and my brother, Nasser and Hadi Gharibdoust, who never ceased to give me encouragement and pray for me in my whole life.

I would like to thank Negar Zare Pakzad, for being exceptionally enticing, angelic and gracious and motivating me during the thesis studies.

I want to express my sincere gratitude to my colleagues, Ahmet Bahattin Ersöz, Ozan Demirel, Erhan Budak, Beyazit Bestami Aydın, Gizem Mestav, Armin Taghipour, Milad Baybordiani and my friends Nima Sohrabnia, Ramin Rouzbar who were there to give me support during my study.

I would also like to show my thanks to Assoc. Prof. Dr. Özgür Kurç for providing dam identification data and structural laboratory technicians, Hasan Metin, Murat Demirel, Osman Keskin, Barış Esen and electronic specialist Salim Azak for their helps during experiments.

I would also like thank to The Scientific and Technological Research Council of Turkey (TÜBİTAK) for supporting me financially during my graduate level education.

TABLE OF CONTENTS

ABSTRACT v
ACKNOWLEDGEMENTS x
TABLE OF CONTENTS xi
LIST OF TABLES xiii
LIST OF FIGURES xiv
LIST OF SYMBOLS xvii
LIST OF ABBREVIATIONS xix
CHAPTER 1 1
INTRODUCTION 1
1.1 Motivation of the Study 1
1.2 Literature Review 4
1.3 Scope and Objectives 13
1.4 Thesis Overview 14
CHAPTER 2 15
SEISMIC ANALYSIS OF A CONCRETE GRAVITY DAM 15
2.1 General 15
2.2 Earthquake Analysis of Gravity Dams (EAGD) 15
2.3 Pseudo-Dynamic Test Method 18
2.4 Gravity Dam Peudo-Dynamic Test Procedure 22
2.4.1 Assumptions 25
2.4.2 Detailed Test Procedure 27
2.5 Analysis Results 30
2.5.1 OBE Analysis 30
2.5.2 MDE Analysis 34
2.5.3 MCE Analysis 36
CHAPTER 3 39
PSEUDO-DYNAMIC TESTING 39

3.1 Materials 39
3.1.1 Binding Materials 39
3.1.2 Aggregate Size 41
3.1.3 Concrete Compaction and Mix Results 42
3.2 Base Modification 43
3.3 Scaled Dam Construction 45
3.4 Test Setup 47
3.4.1 Loading Members 47
3.4.2 Instrumentation 49
3.5 Pseudo-dynamic Test 51
3.5.1 OBE Experiment 51
3.5.2 MDE Experiment 54
3.5.3 MCE Experiment 57
3.6 Sliding Analysis 60
3.7 Pushover Experiment 64
3.8 Identification of dynamic properties of the specimen 67
3.9 Strain Gauges 70
3.10 Comparisons with a Companion Specimen 71
CHAPTER 4 75
CONCLUSIONS 75
4.1 Summary of Results 75
4.2 Conclusions 75
Conclusions drawn based on the test results are given below: 75
REFERENCES 77
APPENDIX A 81

LIST OF TABLES

TABLES

Table 2-2-1 Scaled details of prototype model dynamic analysis (OBE) 30
Table 2-2 Error Margins for M, V and σ in Case of Different Mass Values (OBE) . 32
Table 2-3 Scaled details of prototype model dynamic analysis (MDE) 34
Table 2-4 Scaled Details of Prototype Model Dynamic Analysis 36
Table 3-1 Binding material chemical composition by weight (Aldemir, 2016) 40

LIST OF FIGURES

FIGURES

Figure 1-1 Top left: Earth-filled Atatürk dam; Top right: Combined Rock-filled and Concrete gravity Keban dam; Bottom left: Deriner arch dam; 3
Figure 1-2 Failure type with varying friction coefficient and critical acceleration Chopra et al. (1991a) 7
Figure 1-3 Pulse duration effect on sliding distance. Tinawi et al. (2000) 9
Figure 2-1 Dam-Water-Foundation system (Chopra et al. 1984) 16
Figure 2-2 Left: Prototype Dam detail, Right: Scaled Dam details. 23
Figure 2-3 Scaled Ground Motions from Left to Right: OBE, MDE and MCE 24
Figure 2-4 Acceleration Spectra for OBE, MDE, MCE motions and the Turkish Earthquake Code 2007 spectrum 24
Figure 2-5 Comparison of the Base Stress between the Scaled and Prototype Models 26
Figure 2-6 29
Figure 2-7 29
Figure 2-8 Illustration of e on M-V diagram (OBE) 31
Figure 2-9 Scaled Specimen Stiffness determination 31
Figure 2-10 The Comparison of Base Shear between the real and scaled analyses ... 33
Figure 2-11 The comparison of Moment between the real and scaled analyses 33
Figure 2-12 The Comparison of Toe Stress between the real and scaled analyses 33
Figure 2-13 The Comparison of Base Shear between the real and scaled analyses ... 35
Figure 2-14 The Comparison of Moment between the real and scaled analyses 35
Figure 2-15 The Comparison of Toe Stress between the real and scaled analyses 36
Figure 2-16 Comparison of Base Shear between the real and scaled analyses 37
Figure 2-17 Comparison of Moment between the real and scaled analyses 38
Figure 2-18 Comparison of Toe Stress between the real and scaled analyses 38

Figure 3-1 Gravel of size 0-3mm 41
Figure 3-2 Pneumatic hand compactor, cylindrical mold, caompacting steel plate... 42
Figure 3-3 Compaction and Curing of cylindrical samples 43
Figure 3-4 Sulphorous paste pot, cap making mechanism; Universal Testing Machine 43
Figure 3-5 Scaled dam monolith platform 44
Figure 3-6 Scaled dam formwork details (dimensions are in mm) 45
Figure 3-7 Scaled dam construction process 46
Figure 3-8 Steel cap details (dimensions are in mm) 47
Figure 3-9 Lateral Load Mechanism 48
Figure 3-10 Vertical Load Mechanism 49
Figure 3-11 Measuring instruments; 1: Lateral LVDTs at base; 2: Vertical LVDT at toe; 3: High precision LVDT (Heidenhain); 4: LVDT attached to steel cap; 5: LVDT attached to dam tip; 6: Strain Gauges installed at dam base 50
Figure 3-12 Strain gauge positions and its close view 50
Figure 3-13 OBE recorded results 52
Figure 3-14 The axial load variation and the pre-stressing effect during the OBE motion 53
Figure 3-15 Crack Propagation (OBE) 54
Figure 3-16 MDE recorded results 55
Figure 3-17 The axial load variation and the pre-stressing effect during the MDE motion 56
Figure 3-18 Crack propagation (MDE) 57
Figure 3-19 MCE recorded results 58
Figure 3-20 The axial load variation and the pre-stressing effect during the MCE motion 59
Figure 3-21 Crack propagation (MCE) 60
Figure 3-22 Base Slip comparison between Analysis and Test under MCE ground motion 63

Figure 3-23 Tip Displacement comparison between Analysis and Test under MCE ground motion 64
Figure 3-24 Pushover recorded results 65
Figure 3-25 Crack propagation (Pushover) 66
Figure 3-26 Scaled dam monolith dynamic properties; Top: Fundamental period variation, Bottom: Damping ratio variation 69
Figure 3-27 Hysteretic damping plot from Megally (1998) 69
Figure 3-28 Principal Strain distributions along the dam base 71
Figure 3-29 Base displacement records for SB and RB specimens during MCE ground motion (Aldemir, 2015) 72
Figure 3-30 Crack propagation during Pushover test (Aldemir, 2015) 73

LIST OF SYMBOLS

$\emptyset_1$	Fundamental displacement
Y_1	Modal coordinate
r_k	Dam displacement
a_g	Horizontal ground acceleration
M_1	Generalized mass
C_1	Generalized damping
K_1	Generalized stiffness
L_1	Generalized earthquake force coefficient
w_s	Weight of the dam per unit height
ζ_1	Fraction of critical damping for fundamental vibration mode
ω_1	Fundamental natural frequency of dam
H_s	Dam height
$\bar{\bar{P}}_1$	Function representing hydrodynamic pressure on upstream face
H	Depth of impounded water
g	Gravitational acceleration
S_n	Pseudo-acceleration ordinate
h_p	Effective height (Scaled dam)
e	Effective height (Prototype dam)
T_1^p	Fundamental vibration period (Prototype dam)
T_1^s	Fundamental vibration period (Scaled dam)
R_r	Constant related to dam-reservoir interaction
R_f	Constant related to dam-foundation interaction
ζ_r	Added damping due to reservoir interaction
ζ_f	Added damping due to foundation interaction
F_{st}	Total hydrostatic load
D_{n+1}	Displacement at time step n+1

V_{n+1}	Velocity at time step n+1
A_{n+1}	Acceleration at time step n+1
K_I	Implicit stiffness matrix
R	Restoring force
K_p	Proportional gain constant
K_i	Integral gain constant
K_d	Derivative gain constant
V	Base shear
M	Turning moment
m	Concentrated mass
F_v	Vertical load
F_h	Horizontal load

LIST OF ABBREVIATIONS

SDoF	Single Degree of Freedom
RCC	Roller Compacted Concrete
CVC	Conventional Concrete
EAGD	Earthquake Analysis of Gravity Dams
PID	Proportional Integral Derivative
OBE	Operational Based Earthquake
MDE	Maximum Design Earthquake
MCE	Maximum Characteristic Earthquake
LVDT	Linear Variable Differential Transducer
SB	Smooth Base
RB	Rough Base

CHAPTER 1

INTRODUCTION

1.1 Motivation of the Study

In the course of modernization in mankind's life style, resources have been of centric concerns. As opposed to continuous search for resources, particularly for water, post-sedentism agrarian society had to have it readily available at households and farmlands. Ancient civilizations especially those in the Middle East are known to construct dams for irrigation and water supply as early as five thousand years ago.

The discovery of the new materials and persistent struggle to optimize the performance and reduce the arduousness of routine tasks, encouraged the development of new tools that ultimately led to industrial revolution. It yielded an increased job market, more income, better healthcare and welfare. In turn, it boosted the population with ever-increasing resource demands. Beside the resources and the workforce, one other factor triggered this regenerative sequence and has been controlling its rate ever since is energy. Everywhere from tool fabrication to machinery operation, energy has played an inevitable role. The required energy has long been extracted from fossil fuels such as coal and oil but as time passed by, these unsustainable sources could not provide the energy that would suffice industrialization nor civilization with a clean environment. In particular, shortly after the ubiquity of electric power utilization for illumination, dams became one of the major supplies. Advances in concrete technology in time contributed to feasibility of constructing dam at the points of watercourse with high fluid pressures that consequently increases the electricity generating capacity of the dam.

Nowadays, despite the availability of other methods of energy production, hydroelectric dams have preserved their significance for many reasons. The conventional fossil fuel reserves may not meet the local demand in all countries. In addition, burning fossil fuels produces carbon dioxide that accelerates global warming thus is not environmental friendly. Nuclear power plants leave nuclear wastes that potentially jeopardize the well-being of the society. Renewable energy sources in general have a common drawback of intermittency. The time the electricity is generated is uncontrollably not the same as the time it is consumed thus, requiring storage for later use. In contrast, hydroelectric dams have the virtue that they can coordinate the electricity generation according to the energy consumption to an appreciable extent and have the option of energy storage through hydro-pumps, perhaps the largest scale storage option.

Dams may serve other purposes such as irrigation and flood prevention that can be of critical importance. Yet in practice, despite their extreme importance, these purposes provides justification for building dams less frequently than the need for energy. Hence water supply and energy generation are the two main reasons for dam construction in most cases.

In years various types of dams are designed and constructed depending on the location, regional demands and available technologies at construction. Dams are generally separated into two main groups of earth-fill and concrete dams where the latter itself is divided to the concrete gravity and arch dam categories. Various types of dams namely the earth-fill, concrete gravity, concrete face rock-fill and arch dams are illustrated in Figure 1.1.

Since dams are very costly to build and have long construction periods, optimization in dam construction technology, led to the emergence of the roller-compacted-concrete dams. Construction costs of RCC dams are approximately 25 to 50 percent less than commonly placed concrete gravity dams (US Army Corps of Engineers, 2006). Lower

cost of the dam construction is by the virtue of several factors including reduced forming, placement, compaction and material quantities costs besides savings resulting from the reduced construction time. RCC dam construction procedure calls for a continuous placement of material leading to very high production rates. Being compared to conventional concrete dams, construction duration for large RCC projects may be reduced by several months to several years (US Army Corps of Engineers, 2006).



Figure 1-1 Top left: Earth-filled Atatürk dam; Top right: Combined Rock-filled and Concrete gravity Keban dam; Bottom left: Deriner arch dam; Bottom right: Çine RCC dam

Due to the considerable impact of dams in human life, it is vital to consider the risks associated with dam damage or failure. The major risks can be human casualties, local fauna and flora destruction, flooding of civilization infrastructures, blackout and water shortage. Earthquake is one of the natural threats for dams. Our knowledge and

experience on the seismic response of dams continuously improves which gives engineers a deeper insight in the design and construction of dams. However, significant number of dams were already built prior to the era our knowledge became reasonably advanced on earthquakes i.e. earlier than 1980's. For instance, seismic hazard was not known with today's precision and construction standards or knowledge about seismic faults were not developed. As a result, the corresponding provisions for probable damage and failure of existing dams is a major area of concern.

There are several reasons for the detailed seismic analysis of dams. First, the probability that an earthquake hits a dam is not negligible especially in countries with high earthquake frequency such as Japan, China and Turkey. Analysis techniques based on advanced numerical methods by using sophisticated computer programs are accessible nowadays more than ever before and can help to uncover the seismic response of dams.

Observations on the seismic response of RCC dam behavior under severe earthquake loadings is relatively scarce. Insufficient experimental data and lack of knowledge on their failure modes further lead to questioning of our ability on the design and assessment of RCC dams. One important difficulty in conducting experiments on dams is the size of test specimens and appropriately applying the gravity and earthquake induced loads via costly centrifuge and shake table apparatus. The goal of this thesis is to improve the experimental data in this area and validating analytical techniques by using scaled dam test results.

1.2 Literature Review

Numerous researchers have investigated the behavior of dams exposed to seismic excitation. A number of experiments were carried out either using the shake tables or

conventional loading by hydraulic jacks. In addition, numerous simulations were conducted to assess reliability of the experimental data or to predict the performance of dams. In the following paragraphs some important studies directly related to this thesis are presented.

A simplified two stage procedure was proposed by Fenves and Chopra (1984) for the elastic analysis and safety assessment of concrete gravity dams. First, a simplified analysis process in which the response considering of only the fundamental vibration mode was estimated directly from the earthquake design spectrum. Subsequently a refined response history analysis procedure for finite element idealization of the dam monolith was carried out where higher modes responses were included. The simplified analysis procedure included the effects of the dam-foundation interaction and of the sediments accumulated at the bottom of reservoir besides the effects of dam-water interaction, also including water compressibility. The vertical ground motion was not included in the analysis since it was less significant. Each monolith was assumed to be supported on a viscoelastic half plane impounding water reservoir with the presence of alluvium and sediments at bottom of the impounding water reservoir. In their research, a comprehensive effect of water reservoir and foundation effects including the damping modifications and the fundamental period change was presented.

In a related line of work Duron (1987) conducted forced vibration field test and finite element analyses on Morrow Point (arch) dam to investigate the dynamic dam-water interactions and water compressibility. In a parallel analyses, frequency response curves for evaluated accelerations and water pressures, also their resonating shapes were compared to predictions from the finite element model. This work yielded a 1.5% damping by the half-power method at full reservoir level for antisymmetric resonances and around 4% for all of three symmetric resonance cases. Probable explanation mentioned for higher damping values in the symmetric response was the included damping associated with water compressibility that was more emphasized in the symmetric case. The researcher concluded that the fit of the numerical results to the

experimental data for the antisymmetric response at full reservoir was slightly better in case of the second antisymmetric resonant frequency of the system where water compressibility was included in his analysis.

Donlon (1989) conducted a seismic test on a scaled gravity dam by using a shake table. His scaled model comprised of a composition of polymer and plaster-based materials. He also controlled the water penetration and the resulting effects on the mechanism or cracking by implementing a plastic membrane and the prevention of water penetration. Polymer-based materials used in the dam base prevented the formation of the cracks in the lower parts of the dam specimen. The observed crack patterns in dam monolith was V-shaped and sloped upward in downstream direction. The researcher observed no failure despite very strong excitations applied on the dam model.

Chopra and Zhang (1991a) studied the earthquake induced base sliding response of the concrete gravity dams by developing analytical procedures. In their research the possibility of estimating the sliding response of flexible dam by analyzing the response of a rigid dam model was investigated. They assessed four possible failure types (sliding or tipping toward downstream or upstream) of gravity dams under seismic excitation. The analyses results indicated that in the presence of full reservoir, the acceleration required to cause downstream sliding of dam was much lower than that of other failure modes that was due to hydrostatic and hydrodynamic loads. However considering empty reservoir upstream tipping was found to be possible. Figure 1.2 exhibits critical acceleration graphs for each failure mode presented in their study. In the figure h, h_d and α represent the water height, dam height and the dam's downstream face inclination slope, respectively.

Danay et al.(1993) studied weak base rock joints to develop an empirical formula for predicting the seismic-induced slip of the concrete. They performed a series of parametric studies on gravity dams based on the "sliding block" concept and the equivalent single degree of freedom system criteria. Proposed formula was validated

by the finite element analysis, and provides a fair prediction of the seismic-induced sliding for all typical sections of concrete gravity dams.

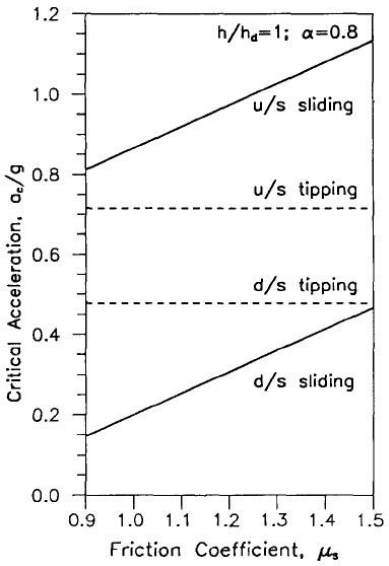

Figure 1-2 Failure type with varying friction coefficient and critical acceleration Chopra et al. (1991a)

Bhattacharjee and Leger (1994) studied two directional static fracture behavior of a full-scaled gravity dam by smeared crack analysis models founded on a nonlinear fracture mechanics (NLFM) approach. A comparison was made between a coaxial rotating crack model (CRCM) and a fixed crack model with variable shear resistance factor (FCM-VSRF), both utilizing secant stiffness method. The research demonstrates that the responses acquired by CRCM appears to exhibit better performance on diminishing the stress-locking phenomenon compared to FCM-VSRF. Nevertheless, crack patterns estimated by rotating crack model were poor on directional bias. On the other hand, FCM-VSRF resulted in a considerably high post-peak structural resistance making it less reliable than CRCM in estimating the post-peak resistance of concrete structures.

Force-vibration experiments were conducted on Outardes 3, an 84 m high concrete gravity dam by Proulx and Paultre (1996). A numerical correlation study employing

experimental data using both two and three dimensional models were conducted. It was indicated that the two-dimensional approach could only predict the fundamental mode of the system while accurate results for the dam-reservoir-foundation interaction including water compressibility can only be achieved by using the three-dimensional model. It should be noted that the conclusions from this research applied to testing conducted on the dam using low amplitude harmonic forced vibrations.

Mir and Taylor (1996) conducted a series of dynamic slip tests on a concrete gravity dam model by using a shake table to investigate the dynamically induced sliding and overturning characteristics of a medium to low height gravity dam monolith cracked at its base. They also performed dynamic finite element analyses of the model using a Lagrangian contact surface algorithm along with Newmark's sliding block approach. Comparison of the results shows that Newmark sliding block approach led to conservative estimates for the seismic induced slip while analytically evaluated sliding response using a finite element contact surface algorithm matched the experimental results. It was also concluded that under full reservoir conditions, downstream sliding may be the only significant failure type of a concrete gravity dam. Moreover, in the absence of large uplift pressure, the probability of the dam overturning about its toe stated to be low. However, considering the empty reservoir condition, the dam may tend to overturn about its heel prior to any slide in the upstream direction.

Ghobarah et al. (1998) carried out an experimental study on a small-scale model of a concrete gravity dam. In the study, two actuators were used to simulate the hydrostatic loads, hydrodynamic and seismic loads respectively through four concentrated point loads. Static load representing the hydrostatic pressure was kept constant while the second actuator applied cyclic loads representing earthquake induced loads. An existing concrete gravity dam monolith was modeled and analyzed. The study included the computation of the dynamic forces on the dam for a specific ground motion and the related force simulation using a number of quasi-static concentrated loads located at the upstream face of the model. Results showed concentrated loads are capable of

approximating the reservoir forces and exhibiting the experimental representation of the dam-reservoir interaction effects with reasonable accuracy.

A number of dynamic experiments on dam models were carried out using a shake table by Tinawi et al. (2000) on four 3.4 m high plain concrete gravity dam models. Test results were compared to finite element simulations using smeared crack model. In their study, numerical simulations of sliding mechanism was conducted using rigid body dynamics with frictional strength drawn from the Mohr-Coulomb criterion. The tensile strength and fracture energy of the concrete were increased by a constant magnification of 1.75 in their simulation results. This dynamic amplification factor was validated by numerical and test (where no cracking was observed) comparison. Their experiments show viscous damping to be between 1% in an un-cracked situation to over 20% in samples with partial cracks. In their series of experiments sliding due to a single triangle acceleration pulse was observed. Sliding was concluded to be dependent on the duration of the pulse, Δt squared. Once the critical acceleration necessary to induce sliding was less than the peak acceleration, pulse duration becomes more important. Effect of pulse duration on sliding distance presented by the authors are shown in figure 1.3.

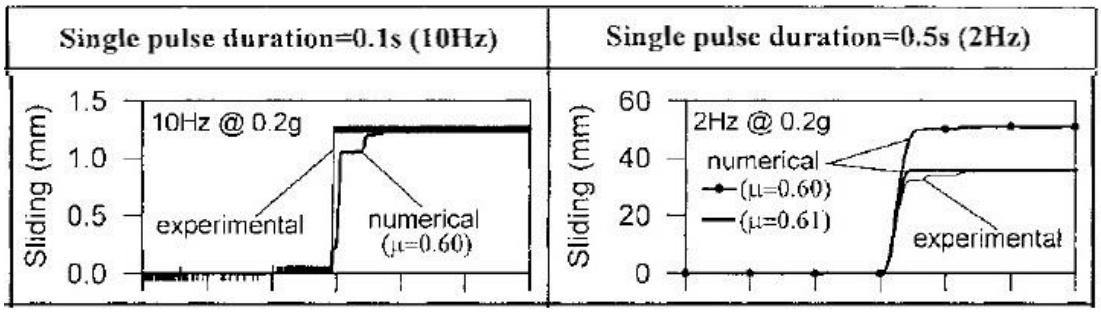

Figure 1-3 Pulse duration effect on sliding distance. Tinawi et al. (2000)

Strain controlled uniaxial tensile and compressive experiments of roller compacted concrete were conducted by Chuhan (2002) to establish the constitutive relationship of RCC. Subsequently, utilizing test data, 200-m high Longtan RCC dam was analyzed

for seismic resistance using the procedure of nonlinear fracture mechanics and the compression-shear failure behavior for concrete. The nonlinear fracture analysis demonstrated that for the full reservoir situation in the static case, the over load factor of 1.20 could be obtained and the upstream heel of the dam was most likely to fail. Moreover, for a high reservoir elevation in the dynamic case, the most vulnerable part of the dam was found to be the upstream heel where cracking initiated at around 0.25g PGA. In addition, the downstream face of the upper region with a slope change was determined to be critical. The cracks on the upstream face were propagated under 0.37g as PGA.

Morin et al. (2002) conducted displacement based shear tests on scaled concrete lift joint samples with varying surface roughness reinforced with an un-bonded post tension cable to study the failure mode of the strengthened dams. These experiments were carried out using shake table and 3.4 m high plain concrete post tensioned concrete gravity dam possessing a cold lift joint about mid-height. Authors made a comparison of test recordings and results from numerical simulations. Experiment results demonstrated that the post-tension cable provides supplementary strength to the joint by applying normal load on the joint and by the cable dowel action. Roughened joints observed to present higher post-tension force owing to the dilatancy phenomenon. Experiments also exhibited that post-tensioning reduced the residual sliding displacements of the joint to a great extent. In account for low frequency record, post-tension force of 2 kN diminished the sliding from 203 to 1 mm. On the other hand, a single post-tension cable placed close to upstream face boosts the upstream rocking response of the upper block. This research showed significant shear displacements under strong earthquakes may induce cable failure at a lower value compared to its uniaxial tensile strength.

For the evaluation of concrete dams' seismic performance, Ghanaat (2004) introduced the failure mode approach. In his approach, safety of the dam was assessed on the basis of potential modes of failure and using the magnitude of stress as a measure of the

performance. He conducted both linear-elastic and nonlinear analyses including the dam-water and dam-foundation interaction effects to observe which failure mode (i.e. overstressing, sliding and joint opening) would occur. In his study the acceptable performance was assessed utilizing the stress demand-capacity ratios, the cumulative duration of stress excursions above various ratios of tensile strength and the spatial extent of the overstressed regions.

Ghanaat (2005) in another study presented analyses and evaluation approach to assess the seismic stability of the Claytor gravity Dam and the potential failure mechanisms. He conducted three types of three-dimensional analyses including linear time-history analysis, post-earthquake static analysis and the nonlinear time-history analysis under MCE to assess stability of the dam. Result of analyses demonstrated that the spillway towers underwent sliding and rocking motions, however these motions would be minimal (i.e. smaller than 0.1 mm sliding) with a least impact on the stability of towers and functionality of the gates. The pier would experience cracking but the cracks would not extend to the whole section due to decoupling of the damaged tower from the pier. Consequently, the pier would remain stable and capable of handling the structure along MCE ground motion.

Uchita et. al. (2005) conducted a dynamic test of a concrete gravity dam monolith exercising a shake-table mounted inside a centrifuge for the first time. In their experiment, a 1/30 scaled dam model of 18 m height was subjected to a harmonic excitation of 167 Hz frequency. Two tests were carried out, on specimens with dry and wet interfaces, under 30 g of centrifugal acceleration. The experiments were interrupted due to the formation of cracks at the foundation. Nonetheless, these tests were used to validate finite element codes. Furthermore, they were the first for the simulation of a realistic loading state during a dynamic test benefitting from the centrifugal acceleration and shaking abilities of the equipment.

A 1/300 scaled model of an arch dam of height 278 m was exposed to three different level of seismic excitation on a shake table by Wang and Li. (2006). In their test, arch dam behavior under seismic overloading was investigated. In the experiment, the contraction joints, partial elastic foundation and the reservoir effects have been simulated. The opening of joints during the strong earthquake reduced the acceleration response and tensile arch stress, subsequently the cantilever stress on downstream ide exceeded the tensile strength and the arch dam responded non-linearly after that point. Material used in the model dam possessed 2.3 times higher strength than the target value and the highest dynamic overloading level was 2.26 times of the seismic design level. The results of the experiment indicated the damage caused a reduction in the natural frequency while the serviceability of the model did not seem to change.

A series of shear and shake table sliding experiments are performed by Rochon-Cyr and Leger (2009) on a 1.5 m high scaled concrete gravity dam with cold lift joints. These experiments were carried out in dry, wet and pressurized conditions. Monotonic shear tests revealed dry dynamic friction coefficient was about 15% smaller than the dry static friction coefficient while a 32% cut-back was observed between the wet static friction coefficient and the wet dynamic friction coefficient. Sudden sliding displacements were initiated in pressurized concrete-concrete interface condition. They applied both sinusoidal pulse and seismic excitation to the specimen and it was indicated that residual sliding was larger for low frequency pulse (2 Hz) than for high frequency pulse (10 Hz). It was also observed that the uplift pressures could diminish vertical force, thus concrete-concrete dynamic coefficient drops from 0.4 to 0.25 leading to higher sliding motion.

In a study carried out by Basili et al. (2011) a nonlinear single degree of freedom model in which dam-water-foundation interaction was considered to obtain the concrete gravity dam base sliding response. Considering a threshold value for the sliding foundation resistance (Mohr-Coulomb yielding criterion including a frictional and a cohesive component was utilized) the nonlinearity was mainly stated to be in the

foundation rock. In this research a nonlinear step-wise dynamic analyses was performed on four case studies representing examples of Italian concrete gravity dams of different heights by employing various seismic excitations. The study concluded that dam seismic residual displacement could be approximated by performing equivalent SDOF system parameters instead of nonlinear dynamic analyses considering the dam height, impounded water level and foundation rock type.

The dynamic failure mechanism of concrete gravity dam during seismic excitation was investigated using a dam section model with a powerhouse, employing a shake-table in a study by Chen et al. (2012). Reservoir and rigid foundation induced effects were the main assumption for this research. Influential factors for the failure of the gravity dam model were analyzed by numerical methods. It was determined that the nonlinear behavior of the model during the experiment matched well with the results. It was stated that the nonlinear effect after the initiation of cracks caused significant changes in the dynamic response under the applied strong motion.

1.3 Scope and Objectives

This thesis is aimed at employing a pseudo-dynamic testing approach that is recently proposed by Aldemir et al. (2015) to study the sliding response of a scaled roller-compacted-concrete gravity dam. Data achieved experimentally and corresponding analyses aims at improving the data base for the dynamic behavior of RCC gravity dams under various earthquake ground motion levels. Dynamic tests were conducted to observe crack propagation patterns and evaluate the effect of inter-layer bonding quality on seismic response. Furthermore, a pushover test is conducted to assess reserve capacity of a scaled dam specimen and its failure mode.

A lift joint with a smooth surface at the dam foundation interface was employed in the tests. Experiments carried out in scope of this thesis are assumed to simulate dams on

smooth foundation interfaces. The primary goal was to assess the change of failure mode of dams constructed on such foundation interfaces from the severe body cracks as reported by Aldemir et al. (2015) to a base sliding mode. Furthermore, the accuracy of the previously proposed sliding model of Chopra and Zhang (1991b) is critically reviewed in light of the test results.

Seismic safety of the Melen dam, a RCC gravity dam, being constructed on the Melen river was investigated throughout this thesis for three earthquake ground motion levels. In the series of experiments carried out in Structural Laboratory of Middle East Technical University, sample dam specimen was subjected to three ground motions of OBE, MDE and MCE levels to evaluate the stability and the seismic safety of the model.

1.4 Thesis Overview

This thesis includes the state of the art pseudo-dynamic test procedure and related experimental recordings. In the second chapter simplified seismic analyses introduced by Chopra et. al. and its common ground with the pseudo-dynamic testing method is described. EAGD analyses conducted on prototype dam considering dam-water-reservoir interactions is explained. A rigorous description of the simplified pseudo-dynamic testing procedure is presented in the third chapter and the outline of procedure is illustrated. Detailed results acquired from a series of analyses performed for the specification of pseudo-dynamic testing variants are presented herein. Subsequently materials used in the scaled dam construction, such as the aggregates and the binding materials are explained. Base modifications and subsequently construction process is described. Then the installment and characteristics of the measuring apparatus are presented. The last chapter is dedicated to discussion of the results, and deriving conclusions by comparing the results within this study by those achieved by Aldemir et al. (2015) and evaluating the slip model of Chopra and Zhang (1991b).

CHAPTER 2

SEISMIC ANALYSIS OF A CONCRETE GRAVITY DAM

2.1 General

Despite the simple geometry of concrete gravity dams, acquiring their seismic response is quite challenging as their analysis requires considering the interactions of dam body, foundation and the reservoir. In the design of concrete and RCC (Roller Compacted Concrete) gravity dams, there exist multiple factors that should be be considered. In a gravity dam, stiffness is distributed throughout the structure in a continuously from its base to top: the inertial forces and vertical loads are distributed along the dam body. These structures are also subjected to lateral forces due to the reservoir hydrostatic and hydrodynamic effects which increase the complexity of the response. In this context, seismic testing if can be designed intelligently, is possible to uncover the fundamental factors affecting the earthquake response of concrete gravity dams.

2.2 Earthquake Analysis of Gravity Dams (EAGD)

In low amplitude seismic excitations dams can remain un-cracked but for high amplitude earthquake excitations dam response is dependent on the crack opening and the respective propagation. In case of dams with vertical contraction joints, the shear force developed during large amplitude motion generally exceeds provided shear capacity and slip may occur between monoliths. As a result monoliths can vibrate independently. For such dams two dimensional, plain stress model of individual monolith can be assumed to yield reasonable approximations (Fenves et al., 1984).

In the concrete gravity dam analysis method developed by Chopra et. al. (1980), a system composed of three substructures was represented with a finite element system for the dam body, the fluid domain, as a continuum of infinite channel with a constant depth, and the foundation rock substructure as a viscoelastic half-plane. Modal displacements induced by seismic excitation were computed by combining their complex frequency responses using the Fast Fourier Transform procedure. The stress responses were consequently computed from the modal displacements. The importance of the effects of the reservoir bottom material on the fundamental mode response of dam was also considered. As a result, in the study of Chopra et al. (1984) this method was presented along with a computer program EAGD for the analysis of concrete gravity dams (Figure 2-1). This program considers the interactions between dam, water and foundation. The effect of sediments accumulated in reservoir base in the vicinity of the dam is also considered. Behavior of the dam, foundation and impounded water is then analyzed in a frequency domain approach. In EAGD, the dam body is modelled by finite number of planar four-node elements. Number of elements can be adjusted considering cross section geometry and size. Dam cross section can be defined as both quadrilateral and triangular elements.

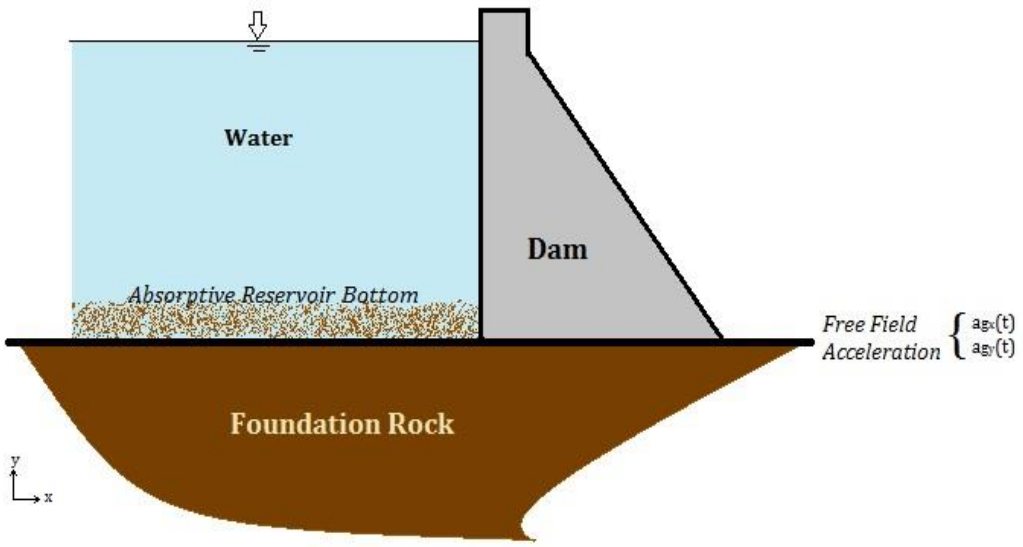

Figure 2-1 Dam-Water-Foundation system (Chopra et al. 1984)

A number of assumptions were employed in the EAGD program. The hydrodynamic effects of water impounded in the reservoir are assumed to be adequately modelled by the two dimensional wave equation. Due to significant effect of water compressibility on the earthquake response of gravity dams, it is included in the calculations considering frequency dependency. The system is analyzed under the assumption of linear behavior for the concrete dam, impounded water and the foundation rock. Consequently, the possibilities of cracking of the concrete or cavitation are not considered. The water impounded in the reservoir is idealized as a fluid domain of constant depth and infinite length in the upstream direction. 2D wave equations are used in analyses with presumed unit weight of 1 ton/m^3 and a presumed pressure wave velocity of 1438.7 m/s.

The foundation rock underlying the dam and reservoir bottom materials is idealized as a homogeneous, isotropic and viscoelastic half-plain. The effect of flexible foundation on the dam body response was considered by the dynamic stiffness matrix of the foundation rock (Chopra et al., 1980). Consequently, the frequency dependent compliance functions are determined for each degree of freedom at nodes located at the flexible foundation boundary for a constant damping value. The hysteretic damping for the foundation rock should be determined before the analytical model formation from site experiments.

A user friendly interface has been developed by (Yücel, 2013) that pre-processes the input data required for EAGD. The raw information defined by the user is converted to a compatible version for EAGD through an –m file. The interface is designed to interact with the user by pop-up notification window in order to prevent entering improper data and other possible execution problems. Furthermore the foundation compliances are calculated for any number of divisions such that a fine mesh could be used for the dam body. With this new version, the mesh division limit (8 elements along the base) is removed. EAGD is utilized in the preparation of the testing protocol assuming the results from it correspond to the “exact” elastic solution.

The prototype dam was modeled as a plane stress system with the 20x25 mesh size on the rigid foundation rock. The modulus of elasticity was taken as 13 GPa with the poison ration of 0.2 with the mass density of 2400 kg/m^3. Such a low modulus of elasticity represents the value commonly used in the design of RCC dams. The hysteretic damping of the model was taken as 5%. No vertical ground acceleration was considered as was discussed previously, however the horizontal ground acceleration data was used from the acceleration data for each ground motion separately.

2.3 Pseudo-Dynamic Test Method

There are two frequently used methods for analyzing gravity dams according to Fenves and Chopra (1985). First one is a refined response history analysis utilizing a semi analytical-numerical technique as explained above. Beside this semi-analytical method, there is a simplified procedure in which dam monolith is represented with an equivalent single degree of freedom system. Corresponding SDoF system was developed in order to exhibit fundamental mode response of gravity dam, consequently making the analysis of gravity dam behavior possible with less complex computations. Single degree of freedom system idealization is the key inspiration utilized herein for the development of a pseudo-dynamic testing approach.

Pseudo-dynamic testing method is more advantageous than the shake table and quasi static methods as it combines the positive sides of the two methods. Testing the dynamic response for specified ground motion which is the most important feature of shake tables is possible in the pseudo-dynamic testing method. Besides it permits experiments on large specimens, precise control and measurement of displacements and forces, easy observation of the damage progression and the probability of halting the test procedure (Molina, et al., 1999).

The foundation of this method is driven from the numerical time integration of the equation of motion where, M and C are respective mass and viscous damping of system, R is restoring force vector, a, $\dot{a}$ are the acceleration and velocity of the single degree of freedom system at the associated time segment.

$$MA + C\dot{A} + R = F$$ **Equation 2-1**

Equation above is a generalization of equation of motion in which F is a general external force vector that includes either equivalent seismic forces or directly applied forces. Numerical algorithm being used in this dissertation is the Explicit Newmark method that is equivalent to the central difference algorithm. It can be represented as follows:

$$MA_{n+1} + (1+\alpha)CV^*_{n+1} - \alpha CV^*_n + (1+\alpha)R^*_{n+1} - \alpha R^*_n = (1+\alpha)F_{n+1} - \alpha F_n$$ **Equation 2-2**

$$D^*_{n+1} = D^*_n + \Delta t V^*_n + \Delta t^2 \left[\left(\frac{1}{2} - \beta\right)A_n + \beta A_{n+1}\right]$$ **Equation 2-3.a**

$$V^*_{n+1} = V^*_n + \Delta t[(1-\gamma)A_n + \gamma A_{n+1}]$$ **Equation 2-3.b**

In these equations D_{n+1} ,V_{n+1} and A_{n+1} represent displacement, pseudo-velocity and pseudo acceleration at time step (Δt) n+1 respectively. The explicit Newmark method is defined by the coefficients:

$$\alpha = 0, \qquad \beta = 0, \qquad \gamma = \frac{1}{2}$$ **Equation 2-4**

As a result the equation of motion at time step n+1 will change as follow:

$$MA_{n+1} + CV^*_{n+1} + R^*_{n+1} = F_{n+1}$$ **Equation 2-5**

Components of explicit Newmark algorithm can be demonstrated as below:

Time Step n (implicit Newmark approximation):	$D^*{}_n = D_n$	**Equation 2-6.a**
	$V^*{}_n = V_n + \Delta t \gamma A_n$	**Equation 2-6.b**
Time Step n+1 (explicit Newmark approximation):	$D_{n+1} = D^*{}_n + \Delta t V^*{}_n + \frac{1}{2}\Delta t^2 A_n$	**Equation 2-6.c**
	$V_{n+1} = V^*{}_n + \Delta t(1-\gamma)A_n$	**Equation 2-6.d**
Time Step n+1 (measured):	$R_{n+1} = R(D_{n+1})$	**Equation 2-6.e**

It is assumed that difference between explicit and implicit forces are small and can be predicted by a linear model:

$$R^*{}_{n+1} - R_{n+1} = R(D^*{}_{n+1}) - R(D_{n+1}) \approx K_I(D^*{}_{n+1} - D_{n+1}) \quad \textbf{Equation 2-7}$$

in which K_I is an implicit stiffness matrix which preferably overestimates the initial stiffness of the structure. Starting from the initial values D_n , V_n , A_n when n=1 (t=0), the successive sequence of algorithm at every time step is mentioned in six stages by (Molina et al., 1999):

Stage 1: Compute at instant n the implicit displacements and velocities D^*_n ,V^*_n using equations 2.6a and 2.6b.

Stage 2: Next, at instant n+1 compute the explicit values of displacement and velocities D_{n+1} , V_{n+1} using equations 2.6c and 2.6d

Stage 3: Impose on the structure the new explicit displacement D_{n+1} and measure the associated restoring force 2.6e.

Stage 4: Increment the step counter n → n+1

Stage 5: Compute the acceleration at new time n from the equilibrium equation

$$A_n = \tilde{M}^{-1}(F_n - R_n - CV_n) \qquad \textbf{Equation 2-8}$$

where,

$$\tilde{M} = M + (\gamma\Delta_t C + \beta\Delta t^2 K_I) \qquad \textbf{Equation 2-9}$$

Stage 6: Repeat preceding steps until the final time is reached.

Experimental section of this thesis is conducted by employing the pseudo-dynamic testing approach overviewed in previous part. General external vector, F, can be presented by multiplication of mass and ground acceleration, a_g, at the same time fraction, with a negative sign. During the pseudo-dynamic testing for each ground excitation a numerical mass value is assigned that will be discussed later. The hysteretic damping of the structure is considered by the physical testing of the specimen. Therefore, the viscous damping in numerical equation is assumed to be zero. As presented in Equation 2.2, equation of motion is formulated and integrated in generalized degree of freedom. At every step of integration the experimental restoring force is statically transformed into generalized force and, once the new generalized displacement is calculated, the target displacement for the transducer on the structure is obtained by kinematic transformation (Molina, et al., 1999).

Computed target displacements in this study are controlled by the Proportional-Integral-Derivative (PID) controller mechanism, then applied to structure by the actuator. In the literature on PID controllers, acronyms are also used at the element level: the proportional element is referred to as the P element, the integral and the derivative elements as I and D elements respectively. P element represents the error at time t, which is the present error. I element is integral of the error up to the instant t, which can be interpreted as the accumulation of the past error. Eventually D element is the derivative of the error at the instant t that can be interpreted as the prediction of the future error. In equation 2.10, E(t) is target variable which is tip displacement

within the scope of this dissertation. Controller synchronizes the target displacement to calculated error and adjusts the displacement accordingly.

$$E(t) = K_p e(t) + K_i \int_0^t e(\tau)d\tau + K_d \frac{d(e(t))}{dx} \qquad \textbf{Equation 2-10}$$

In PID controller formula, equation 2.10, K_p is proportional gain constant, K_i and K_d are respective integral and derivative gain constants. Present time is shown by t while τ is time integration variable used in iterations and e(t) is the gap between the target displacement and the measured displacement. Feedback information (measured displacement) in the conducted test was provided with the high precision displacement transducer, Heidenhain.

2.4 Gravity Dam Peudo-Dynamic Test Procedure

Pseudo-dynamic testing has been previously used in various setups (Takanashi 1982, Mahin et al. 1985, Nakashima et al 1992, Kurt et al. 2012) . In the case of concrete gravity dam testing, there exists only one proposed method (Aldemir, et al., 2015).The experiment within scope of this thesis is conducted similarly with one key difference at dam-foundation interface. The study by Aldemir et al. (2015) had a rough concrete foundation interface, whereas the test specimen in this thesis had a smooth interface without any roughening. Except for the properties of the dam-foundation interface, the remaining approach was kept the same as in Aldemir et al. (2015).

As discussed in the previous subchapters, two dimensional behavior of the dam monolith can be used to simulate the reaction of the whole structure under the seismic effects. Within the experimental scope of this thesis, a scaled sample of the Melen dam's highest monolith has been constructed. Considering the "V" shape of valley, the highest monolith of dam is located at the middle of the construction, with a height and width of 120 m and 15 m, repectively. Melen dam is being constructed over Melen

river, in Sakarya province, Turkey, in order to provide the fresh water demands of Istanbul.

Considering the limitations in the METU structures laboratory, a 1/75 scaled sample of the monolith was built and used throughout this thesis. Accordingly a compression factor of $1/\sqrt{75}$ is employed in time segments to recover the effects of scaling. A schematic view of both the prototype and the scaled dam is represented in Figure 2.6 with the hydrostatic, hydrodynamic and the distributed static loads respectively. The scaled cross-section of dam is idealized as a distributed stiffness system up to its critical height (h_p) where a concentrated mass (m) is located. Choosing proper values for the critical height and the concentrated mass leads to similar base stress demands for the system that was obtained from the EAGD analysis under seismic excitation.

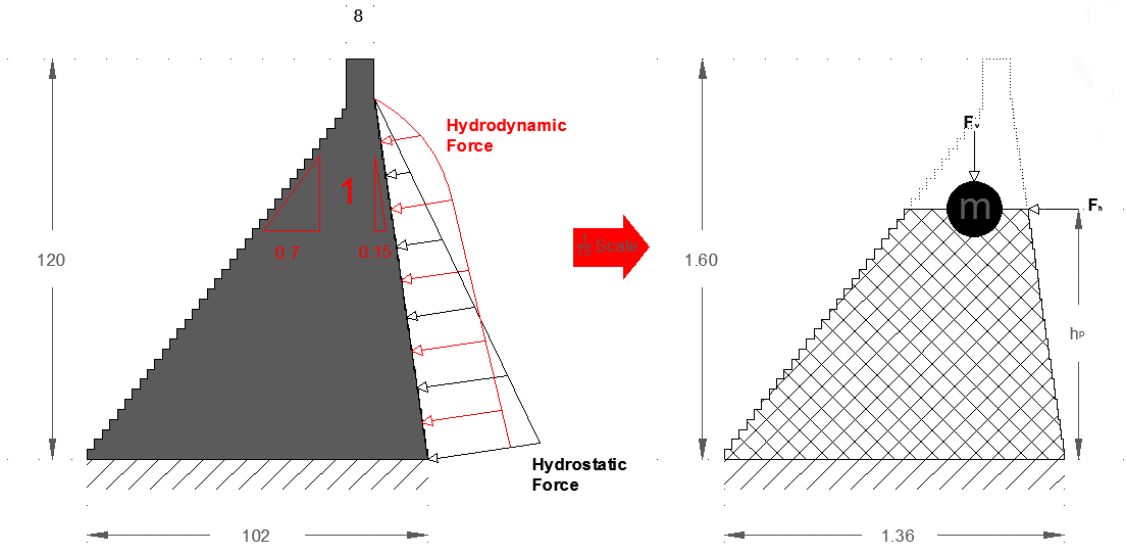

Figure 2-2 Left: Prototype Dam detail, Right: Scaled Dam details.

(All units are in meters)

During the design of dam structure three ground motions that are compatible with the site specific response spectrum were developed (Akkar, 2010). Each of these three ground motions corresponds to different hazard level. The operational based earthquake (OBE) is the earthquake for which the structure is designed to remain operational, with the minimal damage following the incident. Among the three ground

motions, operational based earthquake is the most likely to occur during design life of the structure with a return period of 144 years. The maximum design earthquake (MDE) is the earthquake that is expected to produce the design level of shaking at the site with repairable damage. The recurrence period of MDE is 475 years. Finally, the maximum characteristic earthquake (MCE) is the largest expected earthquake on site. During the MCE earthquake, severe damage may occur on the monolith, however collapse cannot be tolerated. The recurrence period of the MCE excitation is taken as 2475 years. The peak ground acceleration for the OBE, MDE and MCE ground motions were 0.11g, 0.16g and 0.33g, respectively. The scaled time histories of the ground motions and the response spectra are demonstrated in Figures 2-3 and 2-4. It can be observed that the site specific response spectrum of the MCE motion is slightly below the TEC due to the location of the dam (i.e. although the dam is located in the first earthquake zone, distance of the dam location to most critical fault yields lower seismic hazard)

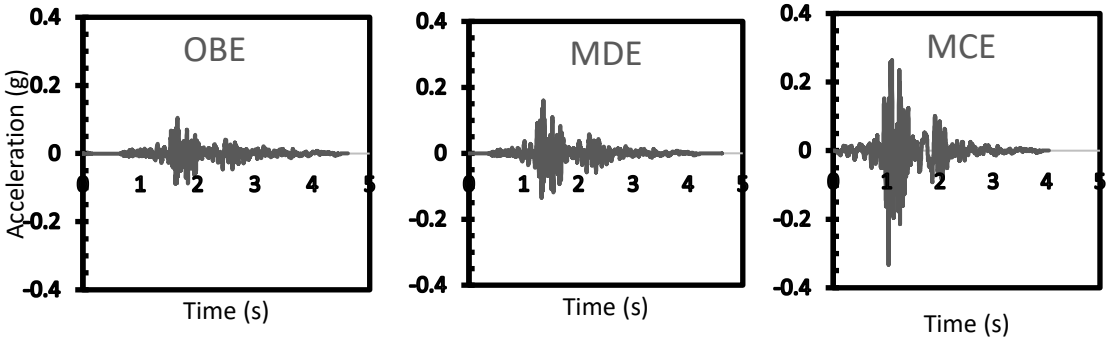

Figure 2-3 Scaled Ground Motions from Left to Right: OBE, MDE and MCE

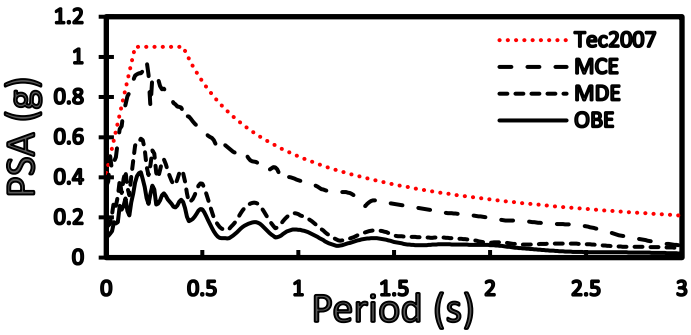

Figure 2-4 Acceleration Spectra for OBE, MDE, MCE motions and the Turkish Earthquake Code 2007 spectrum

2.4.1 Assumptions

In the testing methodology, the hydrostatic and inertial forces are assumed to occur at a point elevated h_p from the dam base. Furthermore, it is assumed that h_p remains fixed throughout the test and does not vary during the ground motion. The validity of this assumption can be verified by referring to M-V diagram. As it will be shown in following section, the effective height of the prototype dam (e) is the slope of the M-V diagram, and consequently h_p is almost the same for all three ground motions (Figure 2-6).

Horizontal component of the exerted load from the inertial and hydrodynamic forces are dictated by the numeric mass m. Numerical concentrated mass (m) of structure is determined through a trial and error approach in which the base shear, overturning moment and the stress value at the dam base on the scaled sample is compared to the respective values of the prototype. Based on the analysis results presented in section 2.5, by choosing the appropriate mass value, stresses at the base of dam turned out to be nearly the same in both the prototype dam and the scaled specimen. The difference in the base shear and moment between the two analyses also did remain within acceptable range. Specified mass can vary in different ground excitations yet remains constant throughout each ground motion. The frequency of vibration during the same ground motion is observed to have insignificant variation for structures containing crack lengths less than 25% of the total base length (Hui, 1995).

By fixing the preliminary factors including: effective height, numerical mass, vertical and lateral loads, the ground motion test is conducted. Consequently dynamic properties of the specimen is identified.

- Since in the single degree of freedom system the body of dam is presumed to be massless, the gravity induced vertical stresses at the base of the dam is simulated by a point load exerted at point m at elevation h_p. In the verification

process, two static analyses were conducted. First analysis was performed on the prototype dam model in order to compute the base stress under gravity and hydrostatic loads while the second analysis was conducted on the scaled model subjected to static point loads with vertical and horizontal components. Vertical component, F_v, simulated the gravity induced loads and the vertical component of hydrostatic load whereas the horizontal component, F_h, simulated the horizontal component of the hydrostatic load. After trying a series of point load combinations, best combination that led to the best match with the initial analyses results turned to be 174 kN and 400 kN for the horizontal and vertical components, respectively. Figure 2-5 exhibits the consistency of principal stress along dam base from the two analyses.

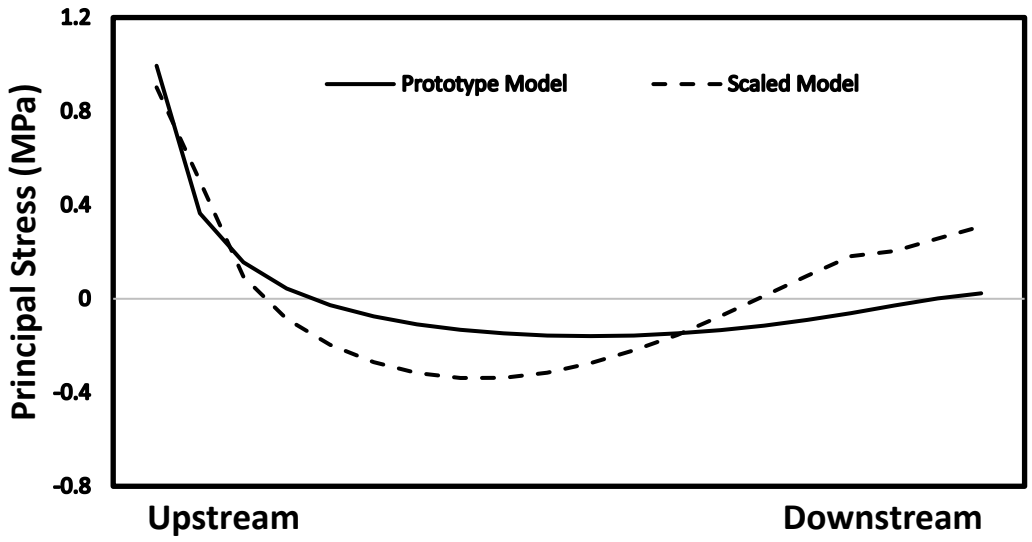

Figure 2-5 Comparison of the Base Stress between the Scaled and Prototype Models

- In the scaling procedure of the test sample, the stress and strain values were unscaled while the fracture energy of the concrete was scaled by scaling the aggregate size. As a result, the fracture process zone of concrete was reduced (Uchita, et al., 2005).

Other assumptions in this study are:

- Tail-water influence was neglected.
- Uplift pressures were not considered.
- The penetration of water into cracks and resultant reduction in the friction forces was neglected.
- Crack propagation in dam body located higher than effective height were not represented and their effect in dam performance were assumed to be insignificant.

2.4.2 Detailed Test Procedure

In the first step of the experiment, a scaled monolith with a single degree of freedom idealization was constructed. Knowing the dimensions of the scaled specimen is a prerequisite for its construction. As discussed in the previous chapter, in order to conduct the pseudo-dynamic testing, the effective dam height (h_p), need to be determined. Consequently a rigorous seismic analysis was performed on the prototype dam model including the dam-water-reservoir interaction. The base shear (V), overturning moment (M) and the fundamental frequency (T) of prototype dam could then be determined.

The moment arm for the system can be determined by establishing the moment versus base shear history diagram and specifying the best fit slope for the response, in other words effective height (e) for prototype dam. Effective height of scaled sample, h_p, was obtained by the multiplication of the prototype effective height with the scale factor.

Once the effective height (h_p) was determined, the scaled specimen was constructed. Afterwards, specimen was subjected to a small lateral load compared to its capacity

such that the specimen remained elastic. In this way the initial stiffness of the specimen was determined. The exerted load included the vertical component that represented the gravity load and a small magnitude lateral load.

Young's Modulus (Modulus of Elasticity) of the single degree of freedom dam model was then adjusted to match the behavior of constructed scaled dam specimen with the measured stiffness.

The other factor to be determined was the numerical mass (m) of scaled sample. This value had to be selected in a way that fundamental period of the scaled dam matched the fundamental period of the prototype dam with full reservoir divided by the square root of the scale factor.

After finding the numerical mass which resulted in in a match between the prototype and the scaled dam periods, a dynamic analysis was conducted on the scaled dam model to acquire the demand parameters time histories such as overturning moment, base shear and toe stresses. These values were expected to be in accordance with respective values gathered from prototype model analysis in EAGD. The errors for the base shear, overturning moment and the toe stress were checked to be in the acceptable limits, otherwise the numeric mass was re-calibrated to minimize the error.

The last factors to be determined were vertical and lateral loads acting on the scaled dam model. A static analysis directed to fix a vertical force (F_v) that leads into similar base stress to that of prototype dam under gravity and hydrostatic loads.

Comprehensive explanation of the experimental procedure is covered above. A summary of the procedure is presented below along with the results. Initially the overturning moment, base shear and the toe stress of scaled dam subjected to point load are obtained to match those values of the prototype dam exposed to the loads. Simultaneously the consistency of the fundamental period of the scaled sample with

the fundamental period of the prototype dam was taken into consideration. A step by step overview of the whole process is given below:

Step 1: Conduct dynamic analysis on the prototype dam model to acquire the fundamental period, overturning moment, base shear and the stress at the toe by using EAGD

Step 2: Determine e from base shear-overturning moment diagram and calculate the corresponding h_p (Figure 2-6)

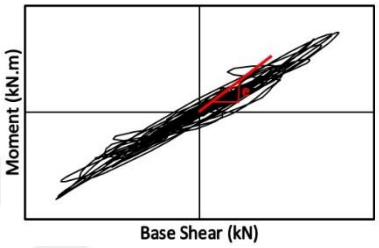

Figure 2-6

Step 3: Construct the specimen and perform initial loading to achieve stiffness, k, of the sample (Figure 2-7)

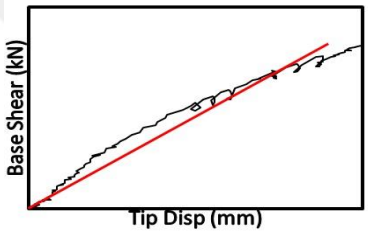

Figure 2-7

Step 4: Select the scaled dam model properties (i.e. Modulus of Elasticity) to match k.

Step 5: Determine m such that the fundamental period of the prototype and the scaled model dyad match each other $T_1{}^s = 2\pi\sqrt{\frac{m}{k}} \rightarrow T_1{}^s = \frac{T_1{}^p}{\sqrt{75}} \pm \delta$

Step 6: Check the accuracy of the resultant M, V, σ from the two analyses conducted with the determined m values. Dissimilarity between the results of the two analyses should be within acceptable range

Step 7: Conduct a static analysis on the scaled model with varying F_v value to achieve the best match for the hydrostatic induced base stress
Step 8: Direct pseudo-dynamic test with details specified in previous steps
Step 9: Identify the dam properties.

Note: In the case of significant errors in step 6, a revised m value was considered and the procedure was continued from step 5 until the errors reduce to an acceptable level.

2.5 Analysis Results

Numerical explanations along with the precise illustrative diagrams of test process is described case by case in sections 2.5.1-2.5.3.

2.5.1 OBE Analysis

Dynamic analysis of the actual dam monolith model with full reservoir exposed to the hydrodynamic and the OBE load case is conducted to obtain the corresponding base shear, moment and stress at toe of dam (Table 2-1).

Table 2-2-1 Scaled details of prototype model dynamic analysis (OBE)

OBE	Base Shear (kN)	Moment (kN.m)	Toe Stress (MPa)
Scaled Max Value	99.96	61.66	1.96
Scaled Min Value	-79.14	-52.99	-1.69

First parameter to be determined is the effective height of prototype dam which is a prerequisite for the scaled dam construction. Target dimensions of the scaled specimen including monolith width and depth, shortly the scale ratio, are chosen considering the limitations of the equipment in laboratory. Effective height of the prototype dam is

established by drawing the base shear versus turning moment. The slope of this diagram represents the effective height of the single degree of freedom system multiplied by the scale factor (Figure2-8).

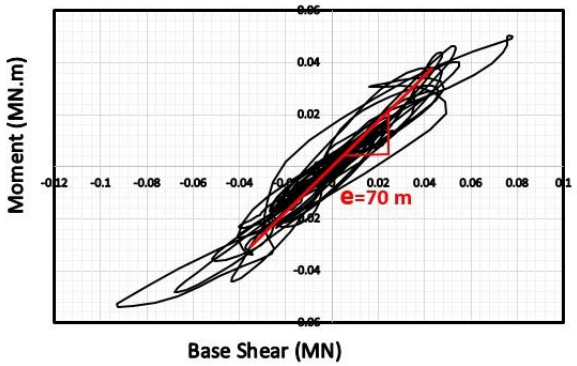

$$h_p = \frac{e}{Scale\ Factor} = \frac{70}{75}$$
$$\cong 0.95\ m$$

Figure 2-8 Illustration of e on M-V diagram (OBE)

Subsequently the specimen was constructed and the initial loading was conducted to obtain the corresponding stiffness. Stiffness value was determined by drawing a line on the tip displacement versus the base shear diagram. In this study the stiffness value is taken to be a secant of force-displacement graph where the force reaches hydrostatic loading level (figure 2-9). The system stiffness was obtained as 684.21 kN/mm from the loading.

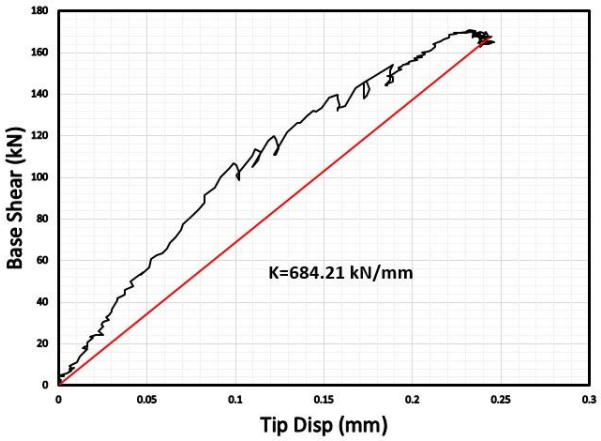

Figure 2-9 Scaled Specimen Stiffness determination

Once the stiffness value was determined, the properties of the scaled dam model had to be calibrated in a way that it exhibits the same stiffness characteristics. Subsequently the modulus of elasticity of the single mass distributed stiffness scaled dam model was determined to be 20.3 MPa by trial and error.

The fundamental period of the prototype dam model was determined to be 0.0584 sec using the EAGD dynamic analysis. A numeric mass value was assigned for the scaled model to exhibit synchronized behavior with the real size model. Corresponding numeric mass value was selected to be 37.5 tons leading to almost no error.

Fundamental periods for the scaled dam model analysis using the established mass quantity agreed with the value of the prototype model; however, this does not necessarily lead to a match between the moments, base shears and the toe stress, thereupon the same check was conducted for latter factors. The errors for the different numeric masses are presented in Table 2-2. The criterion in selecting m as 37.5 tons was a selection based on the optimized combination of errors with the priority of the least error in the fundamental vibration period. As tabulated below, the variation of stress at peak points is within 10% while the overturning moment and the base shear contain up to 28% error in their peaks. Time history responses for M, V and σ_{toe} was also compared and illustrated in Figures 2.10 to 2.12. The selected numerical mass of 37.5 ton was the best match for the fundamental period and the maximum principal tensile stress.

Table 2-2 Error Margins for M, V and σ in Case of Different Mass Values (OBE)

		OBE						
	mass	period	V_{max}	V_{min}	M_{max}	M_{min}	σ_{max}	σ_{min}
Errors	20	25.92	45.28	31.39	15.72	2.66	26.85	15.87
	30	25.92	28.60	3.69	9.96	36.65	4.58	18.20
	35	25.92	35.93	19.43	**1.32**	**14.32**	14.52	**1.28**
	37.5	**0.00**	27.01	9.74	12.41	28.06	**2.54**	10.70
	40	0.64	14.19	**4.13**	32.15	47.74	14.69	27.82
	45	2.51	**6.69**	26.42	64.32	79.36	42.88	55.22

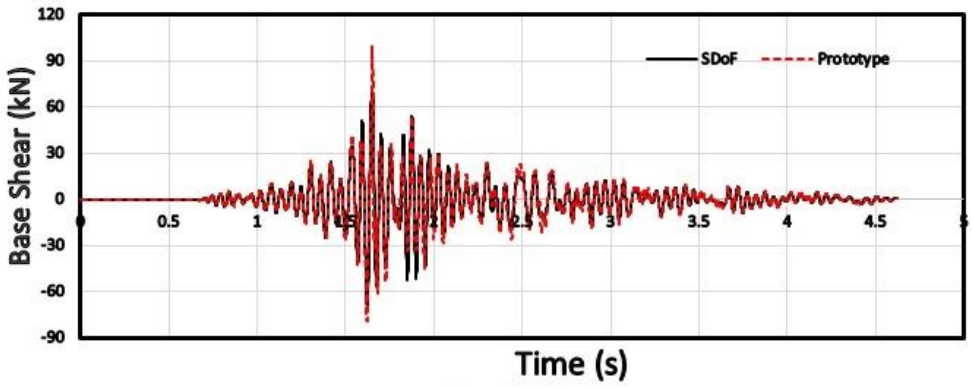

Figure 2-10 The Comparison of Base Shear between the real and scaled analyses

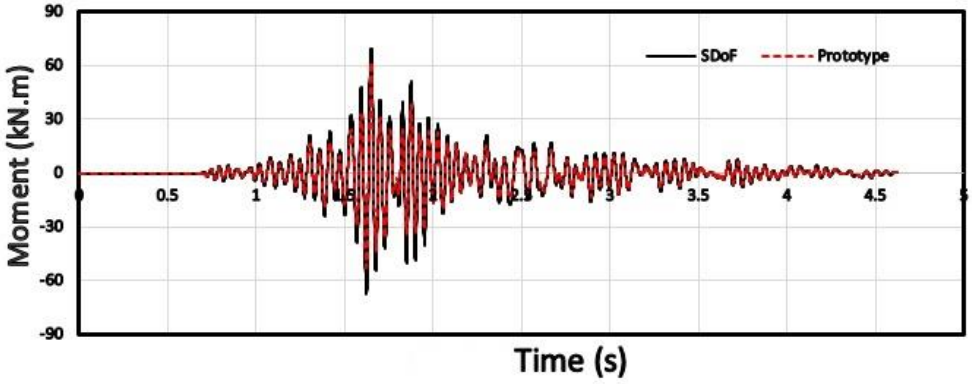

Figure 2-11 The comparison of Moment between the real and scaled analyses

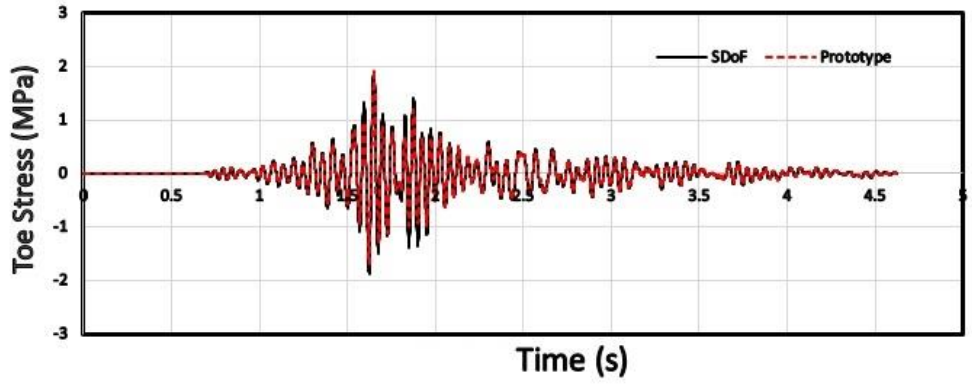

Figure 2-12 The Comparison of Toe Stress between the real and scaled analyses

As it is visible from the diagrams above, the analyses results of the scaled single mass model and EAGD are in perfect match for the OBE motion.

The vertical external force, F_v, that is necessary to reproduce the base stresses similar to that of the prototype model was computed through a static analysis as 400 kN. The same value was used for the MDE and MCE ground motions.

2.5.2 MDE Analysis

Analogous to the test procedure for the OBE ground motion, first a dynamic analysis was performed on the prototype dam model to achieve M, V, σ values and subsequently effective height (Table 2-3).

Table 2-3 Scaled details of prototype model dynamic analysis (MDE)

MDE	Base Shear (kN)	Moment (kN.m)	Toe Stress (Mpa)
Scaled Max Value	147.29	90.01	2.87
Scaled Min Value	-114.37	-76	-2.39

Analysis results demonstrated that M-V diagram's slope in case of the MDE motion did not vary significantly compared to the OBE ground motion. Therefore for simplicity in laboratory installation effective height value was taken to be 70 m.

Maximum design earthquake scenario was conducted on the same specimen, thus the stiffness value, k, was assumed to remain constant as in the OBE motion. Consequently, having no structural damages, calibrated specifications of the scaled dam monolith model employed in the OBE test were remained fixed.

Prototype model fundamental period in case of the MDE motion was obtained as 0.0567 sec. This called for a different numeric mass to be implemented in the scaled model. A trial and error procedure ended up in mass value of 40 tons where fundamental period error turned up to be 0.6%.

Base shear, moment and toe stress time histories carried out from two analyses were put together in the same frame aimed at facilitating the comparison (figures 2.11-2.13).

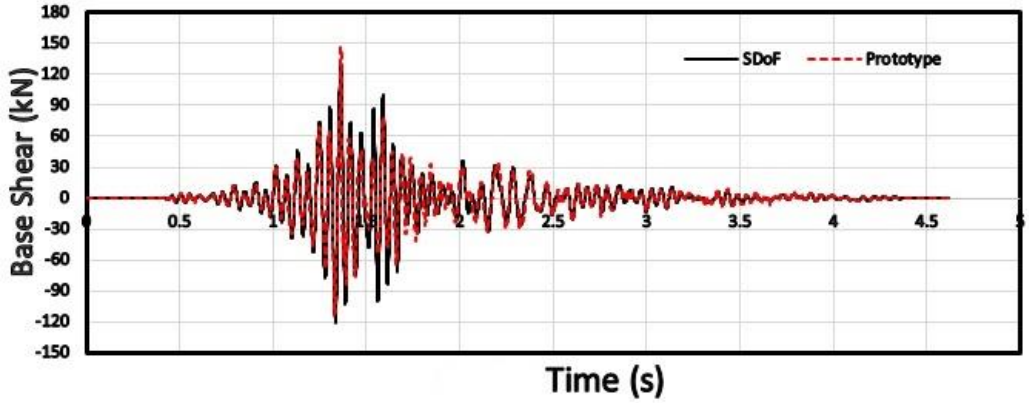

Figure 2-13 The Comparison of Base Shear between the real and scaled analyses

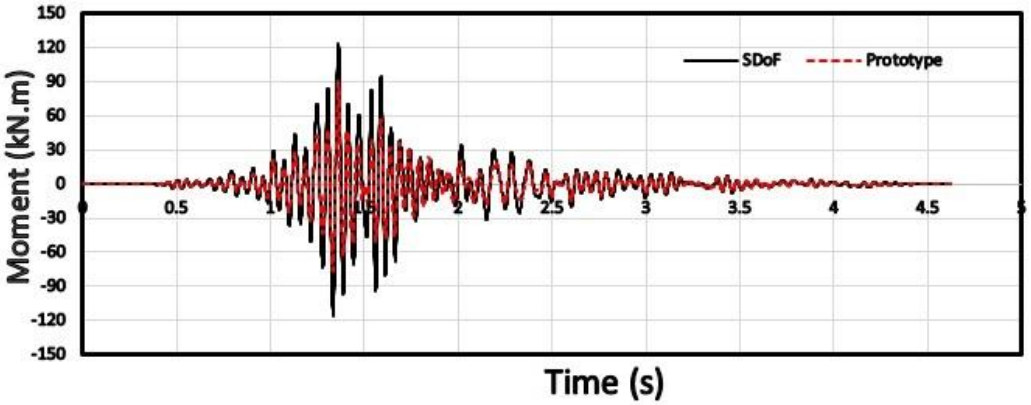

Figure 2-14 The Comparison of Moment between the real and scaled analyses

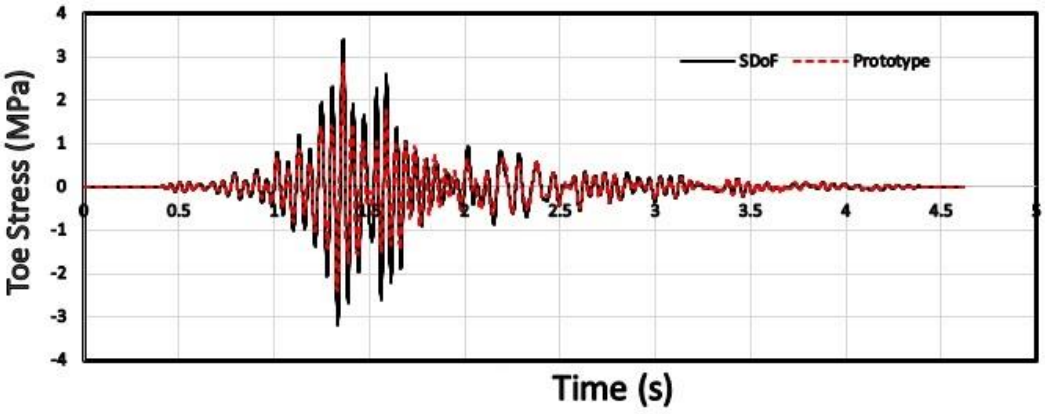

Figure 2-15 The Comparison of Toe Stress between the real and scaled analyses

2.5.3 MCE Analysis

Dynamic analysis on the prototype dam under the MCE motion was carried out with a slight change compared to the two other cases. In order to inspect the dam behavior under large lateral loads with higher resolution, analysis time steps that was selected as 0.01 sec in the two other cases was decreased to half, i.e. 0.005 sec. Peak demand values during MCE ground motion is presented in Table 2-4.

Table 2-4 Scaled Details of Prototype Model Dynamic Analysis

MDE	Base Shear (kN)	Moment (kN.m)	Toe Stress (Mpa)
Scaled Max Value	270.94	165.85	5.53
Scaled Min Value	-216.45	-164.28	-5.10

The M-V diagram for the real size dam model under the MCE motion demonstrated a similar slope to the MDE and the OBE motions. This allowed performing the MCE test utilizing the same test specimen.

The MCE ground motion scenario, in continuation of the two other ground motions, was conducted on the same scaled specimen. Observing no major structural damage,

the stiffness of the sample is assumed to be the same as in the OBE motion. Consequently, the calibrated scaled model in the OBE ground motion was used here as well.

Calibration of the numerical mass was performed for the MCE case by a similar approach to the two other ground motions. Fundamental period of the real size dam under the MCE excitation was 0.0706 sec. The mass value was selected as 55 tons based on the comparison discussed previously. The time history comparisons between the SDoF analysis and the prototype model are presented in Figs 2.16-2.18. A good agreement both in the waveform and the peak values can be observed. As will be shown in chapter 3 this specimen in fact exhibited base sliding. The experimentally observed behavior was therefore different than those presented in Figures 2.16-2.18. However, the validity of the test parameters and results will be confirmed with detailed base sliding analysis later in Section 3.6.

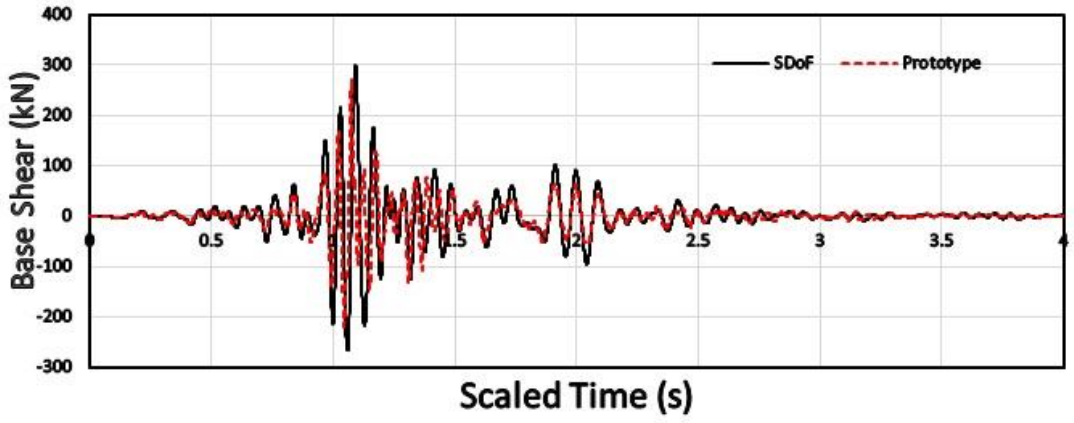

Figure 2-16 Comparison of Base Shear between the real and scaled analyses

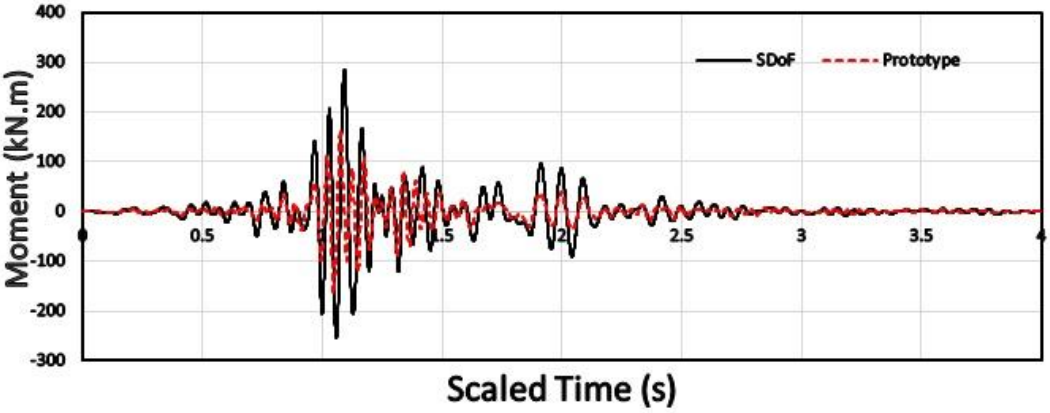

Figure 2-17 Comparison of Moment between the real and scaled analyses

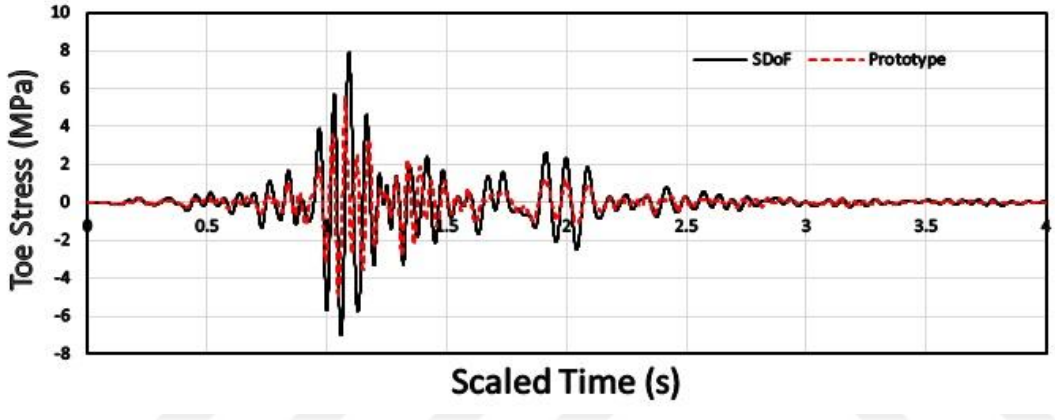

Figure 2-18 Comparison of Toe Stress between the real and scaled analyses

The same vertical, F_v, and lateral, F_h, point loads were employed in the MCE motion pseudo-dynamic experiment. Peak acceleration in the MCE motion was found to be 3 times larger than that of the OBE ground motion, therefore its impact on the scaled dam was expected to be much higher than two other cases. The critical displacement at base of the dam structure, as was expected, occurred for this excitation.

Based on the aforementioned calibrations, the testing procedure was established and the numerical mass was selected as 37.5, 40 and 55 tons for the OBE, MDE and MCE motions, respectively. The results of the tests conducted using the procedure explained above are presented in the next chapter.

CHAPTER 3

PSEUDO-DYNAMIC TESTING

3.1 Materials

Ingredients required for the construction of the scaled dam monolith and their specifications are overviewed in this section. The properties of the binding material, the types of aggregate and the concrete mixture components and their ratios are described herein.

3.1.1 Binding Materials

Dam body was constructed from roller compacted concrete (RCC) composed of cement and fly ash as binding materials. Cement type CEM-I, also known as Portland Cement, was selected as its chemical composition suits dam construction and it is widely available. Fly ash was included in the mixture in order to keep the hydration heat low as high hydration heat in mass concrete may cause undesired cracks. Fly ash properties should comply with the recommended limits by the corresponding standards. Chemical composition for the binding materials published by the Turkish Cement Manufacturers Association, TCMA, is used to compare and choose the appropriate fly ash type (Aldemir, 2016). Components of the cement paste used in the scaled specimen are explained in Table 3-1.

Table 3-1 Binding material chemical composition by weight (Aldemir, 2016)

Chemical Composition	Cement % by Weight	Cement ASTM C150 Limit	Fly ash % by Weight	Fly ash ASTM C150 Limit
SiO_2	18.30	-	63.79	-
Al_2O_3	4.27	-	19.04	-
Fe_2O_3	4.10	-	6.76	-
CaO	62.20	-	1.68	-
MgO	1.29	Max. 6.0	1.65	Max. 6.0
SO_3	2.78	Max. 3.0	0.30	Max. 3.0
Na_2O	0.18	-	1.11	-
K_2O	0.60	-	2.18	-
Equivalent Tot. Alkali (Na_2O+0.658 K_2O)	0.57	Max. 6.0	2.54	-
Free CaO	-	-	0.14	-
Cl^-	0.0102	Max. 0.1	0.0067	-
Reactive CaO	-	-	0.31	-
Density	-	-	2.34ton/m^3	-
2-Day Comp. Strength	19.2 MPa	Min. 12.0	-	-
7-Day Comp. Strength	36.1 MPa	Min. 19.0	-	-
28-Day Comp. Strength	48.7 MPa	Min. 28.0	-	-
Initial Setting Time	235 min	Min. 60.0	-	-
Final Setting Time	445 min	Max. 600.0		
Retained 45 µm sieve	-	-	20.6	Max. 34.0
28-Day Strength Activity Index	-	-	78.0	Min. 75
90-Day Strength Activity Index	-	-	90.2	Min. 75

The proportions of the binding material are designed following the recommendations of ACI 207 (1999) where the cementitious material amounts for a target compressive strength value at a specific age of concrete such as 7th, 28th, 90th day and 1 year is illustrated. In the experiment fulfilled in scope of this thesis, fly ash-cement mix was designed so that fly ash forms 44% of the binding material.

Minimum water cement ratio had to be provided so that the consistency of the paste was self-supporting. Besides an upper limit for the water ratio was assigned to prevent cavities and excess water evaporation which results in the formation of cracks. Water ratio in water-cementitious material is set to be 41% in accordance with ACI 207 (1999).

3.1.2 Aggregate Size

The experiment conducted on the scaled specimen requires the adjustment of the aggregate sizes. The fracture energy of the concrete must be scaled by the sample scale factor, 1/75. Therefore, the fracture process zone of the concrete had to be reduced to decrease the fracture energy. To achieve this goal, aggregate size was reduced to 1/75 portion of the aggregates employed in the prototype model. Consequently the gravel, crushed stone, of 0-3 mm grain size was selected for the concrete mixture (Aldemir, 2016).



Figure 3-1 Gravel of size 0-3mm

3.1.3 Concrete Compaction and Mix Results

Compaction of RCC dam lifts are conducted by vibrating rollers in actual dam construction. During the experiment, the compaction was carried out by using a pneumatic hand compactor in the laboratory environment such that it generates the same compaction energy per second as the one in a real size dam. Concrete samples were provided for the laboratory strength check in 7th and 28th days. These samples were cylinders of size 150x300mm and they were molded and compacted in three layers of 100mm thickness. After casting of each layer, it was compacted by 50mm thick steel plate that was attached to a pneumatic hand compactor. Subsequently, the samples were dismantled and cured under a wet blanket until the day of testing. Related illustrations are presented in Figures 3.2 and 3.3.



Figure 3-2 Pneumatic hand compactor, cylindrical mold, caompacting steel plate

Prior to testing of the samples, their top and bottom faces were flattened by some sulphurous material as cap in order to idealize the axial compressive test. The compressive strength of sample at the 7th day was recorded as 13.5 MPa, while on the 28th day, the experiment day, it reached to 20.4MPa. Compressive tests were carried out in the Materials Laboratory of Civil Engineering Department, METU by universal testing machine with a capacity of 3000 kN. Capping mechanism and the universal testing machine is illustrated in Figure 3.4.



Figure 3-3 Compaction and Curing of cylindrical samples



Figure 3-4 Sulphorous paste pot, cap making mechanism; Universal Testing Machine

3.2 Base Modification

Pseudo-dynamic seismic testing on the scaled roller-compacted-concrete dam monoliths conducted in Civil Engineering Structural Mechanics Laboratory of the

Middle East Technical University within the scope of the research program, Aldemir (2015) conducted three tests on a roughened foundation with three different concrete mix designs. The dam specimen constructed under scope of this study was constructed on a smooth foundation. The smooth foundation interface was attained by rubbing the fine sandpaper (P100) which provided the roughness of less than 0.1 mm.

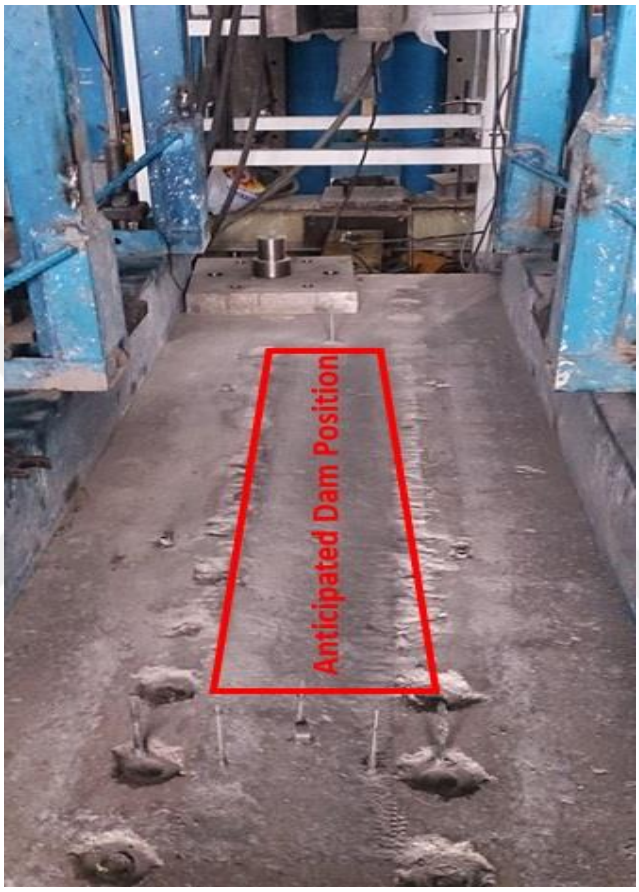

Figure 3-5 Scaled dam monolith platform

Main idea behind the smooth base interface was to observe the effect of the base roughness on the failure mode of RCC dams. In previous experiments conducted by Aldemir et al. (2015), the dam monolith failed through severe cracking in the body without any significant base sliding. The smooth base condition in the experiment

resembles a weak foundation interface in the actual construction that can easily separate from the dam base during seismic shaking.

3.3 Scaled Dam Construction

A formwork was designed and constructed to place the concrete in lifts. The formwork for scaled RCC dam monolith included two steel panels of similar dimensions (height and length) as the scaled dam monolith covering the two sides of the scaled specimen. These panels were connected to each other via small steel plates implemented from bottom to top. These plates, with dimensions of 50mm high and 200 mm length, were placed in a sequence after the completion of the compaction of each layer.

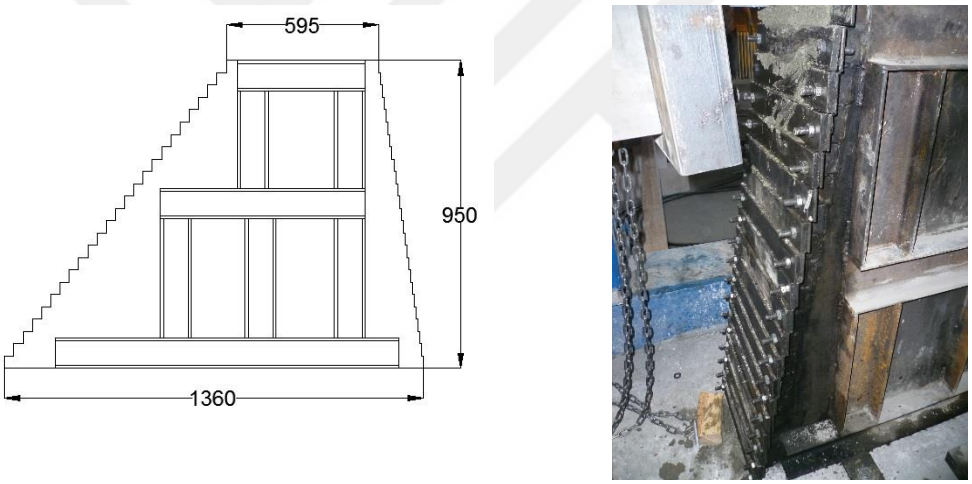

Figure 3-6 Scaled dam formwork details (dimensions are in mm)

Once two steel panels were located at the planned position and the initial segments bolted to hold the form firmly, the first layer of concrete was laid and compacted. The compaction task was performed by a 200mmx200mm steel plate attached to a pneumatic hand compactor described previously. Immediately after the completion of the compaction, the following layer was placed, compacted and this process was continued until the height of 700mm. From that point on the conventional concrete with a compressive strength of 39.1 MPa was poured and vibrated (Figure 3.7).



Figure 3-7 Scaled dam construction process

As the scaled dam sample was planned to undergo high axial and lateral loads, attaching the hydraulic piston to RCC monolith directly would result in the localization of damage at the loading point. Therefore both the lateral and vertical loads were designed to be transmitted to the specimen through a steel cap (Figure 3.8). The steel

cap, specifically designed for this purpose, was encased in the conventional concrete portion of the dam.

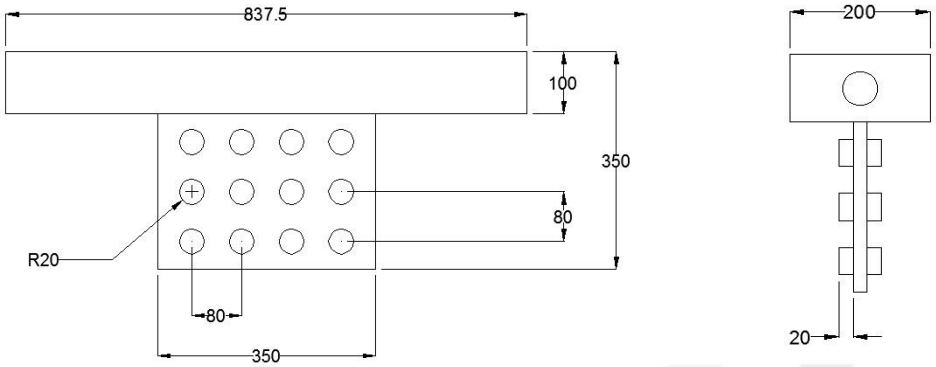

Figure 3-8 Steel cap details (dimensions are in mm)

Formwork was kept on the specimen for 3 days until the concrete gained its strength. Subsequently, the molds were dismantled and a wet burlap was wrapped around the specimen and watered frequently to assure proper curing. Finally, prior to the experiment a thin layer of lime paste was applied around the dam specimen to give a white color in order to assist the observation of the propagated cracks during the experiment.

3.4 Test Setup

3.4.1 Loading Members

While the specimen gained its strength, the test setup was assembled. The setup consisted of a lateral load actuator and a vertical hydraulic jack. The lateral actuator was pin connected to a rigid retaining wall from one end and was connected to the scaled dam from the other end via another pin (Figure 3-9). Lateral actuator with a capacity of 70 tons was used for the seismic experiments and during the pushover test.

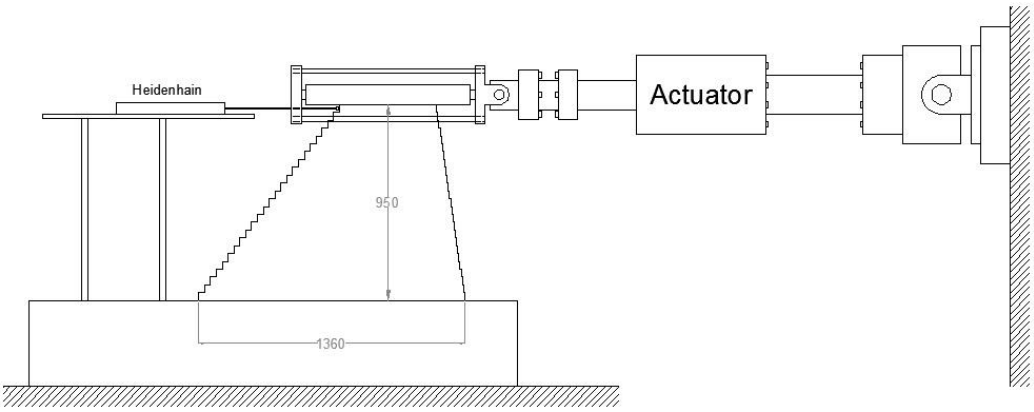

Figure 3-9 Lateral Load Mechanism

In order to set the vertical loading system, initially two steel frames were positioned at both sides of the specimen, then a strong built-up steel cross-beam was positioned on top of dam which had the responsibility of transferring the axial load induced by the hydraulic pistons to the specimen. At both sides of specimen, two steel rods were pinned to the foundation from one end and passed through the built-up section, bolted to the hydraulic pistons at the other ends. Pistons were used to produce tension in rods and resultant force was transmitted, via the built-up section, to the scaled dam specimen as compression and pushed it towards foundation. This pre-stressing task was conducted in order to provide the base stress at the scaled model that was equal to the base stress induced by the hydrostatic loads on the prototype model.

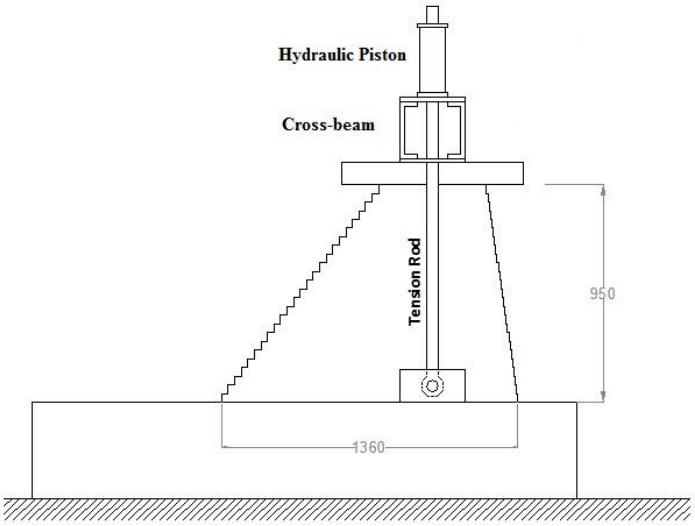

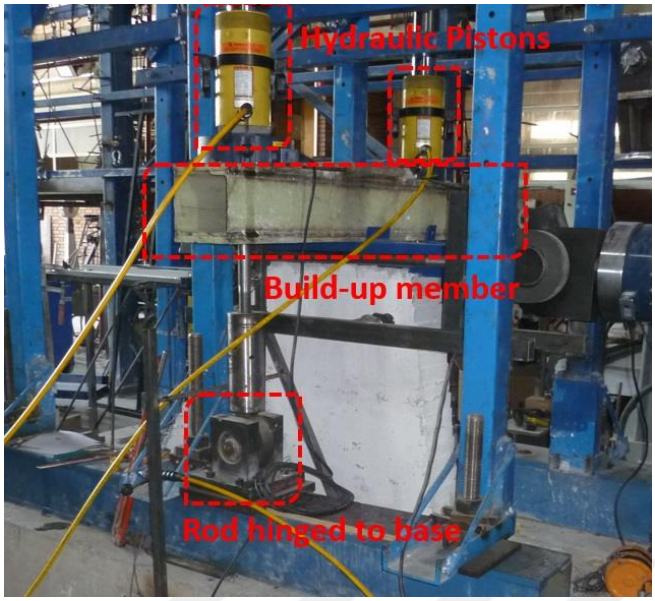

Figure 3-10 Vertical Load Mechanism

3.4.2 Instrumentation

The variation in loading was recorded by using three different load-cells. These load-cells were installed between the pistons and the specimen at various locations to measure the reactions. In addition to these, a built-in load-cell was present along the lateral actuator. This latter load-cell's data was recorded with a different data acquisition system.

Displacements during the experiments were recorded by Linear Variable Differential Transducers (LVDTs), which were capable of recording displacements with high precision. They were installed in both the upstream and downstream of the dam monolith in order to check the variation of displacements. In each side three horizontal and one vertical LVDTs were installed. Vertical one was installed to measure the uplift at the toe. Moreover three LVDTs were attached at the dam top to record top displacements. A high precision LVDT (accuracy of ±10 μm) was used to control the feedback displacement for the pseudo-dynamic system. One of the two other LVDTs was attached to the steel cap and the other one was connected to the upper part of the

dam as shown in Figure 3-11. Furthermore, at the base of the dam monolith strain gauges were attached. These strain rosettes were used to determine principal strains (Figure 3.12). Strain rosettes were bonded to the dam base at 20 cm intervals except for the dam toe (upstream) where first and second gauges were placed 10cm apart from each other. The measuring constituents attached to specimen are demonstrated in detail in Fig 3.11.

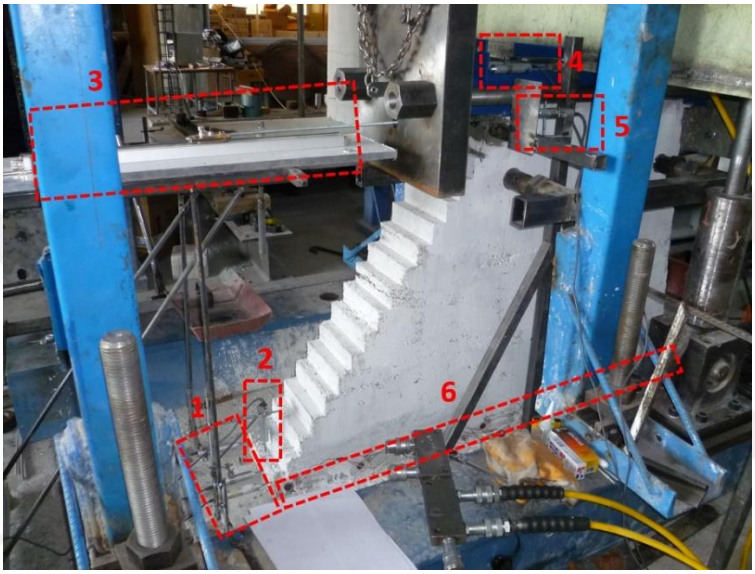

Figure 3-11 Measuring instruments; 1: Lateral LVDTs at base; 2: Vertical LVDT at toe; 3: High precision LVDT (Heidenhain); 4: LVDT attached to steel cap; 5: LVDT attached to dam tip; 6: Strain Gauges installed at dam base

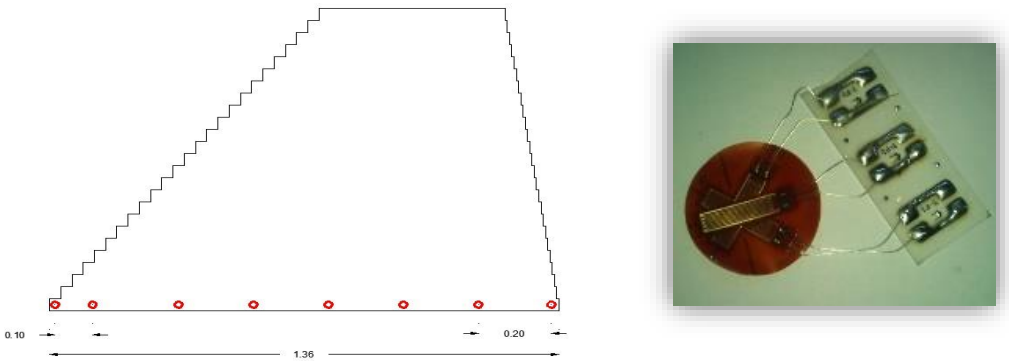

Figure 3-12 Strain gauge positions and its close view

3.5 Pseudo-dynamic Test

This section is dedicated to the experimental results and their discussions. Force demands and the recorded displacements are presented along with the pictures of the dam monolith during testing. Following the pseudo-dynamic tests at three different hazard levels, a pushover test was conducted to determine the reserve capacity of the dam. For the pseudo-dynamic test, as explained in previous chapters, initially the dam was subjected to a vertical load of 400kN in order to simulate the gravitational forces. Then, before the application of the seismic loads the dam was loaded with 174 kN of lateral load at its effective height, h_p, to mimic the application of hydrostatic forces. Subsequently, using the rest of the LVDTs the pseudo-dynamic tests were conducted for OBE, MDE and MCE motions respectively. The results for each ground motion is presented in following sections.

3.5.1 OBE Experiment

Operational base earthquake (OBE) with the peak acceleration of 0.11g was applied to the scaled dam model and the dam behavior was recorded at 0.5 sec intervals. During this ground motion, almost no base sliding was observed (Figure 3-13). Throughout the OBE ground motion, no base cracking occurred. The first crack with 0.75 mm width propagated along the steel loading cap as shown in Figure 3-15. A second crack with a width of about 25 mm was observed along the vertical direction. The third crack, which occurred at the interface of the RCC and the CVC layer had a width of 0.4 mm and extended to about 10 cm. None of these cracks caused a deviation from the linear elastic response as none were at the critically stressed location (i.e. base).

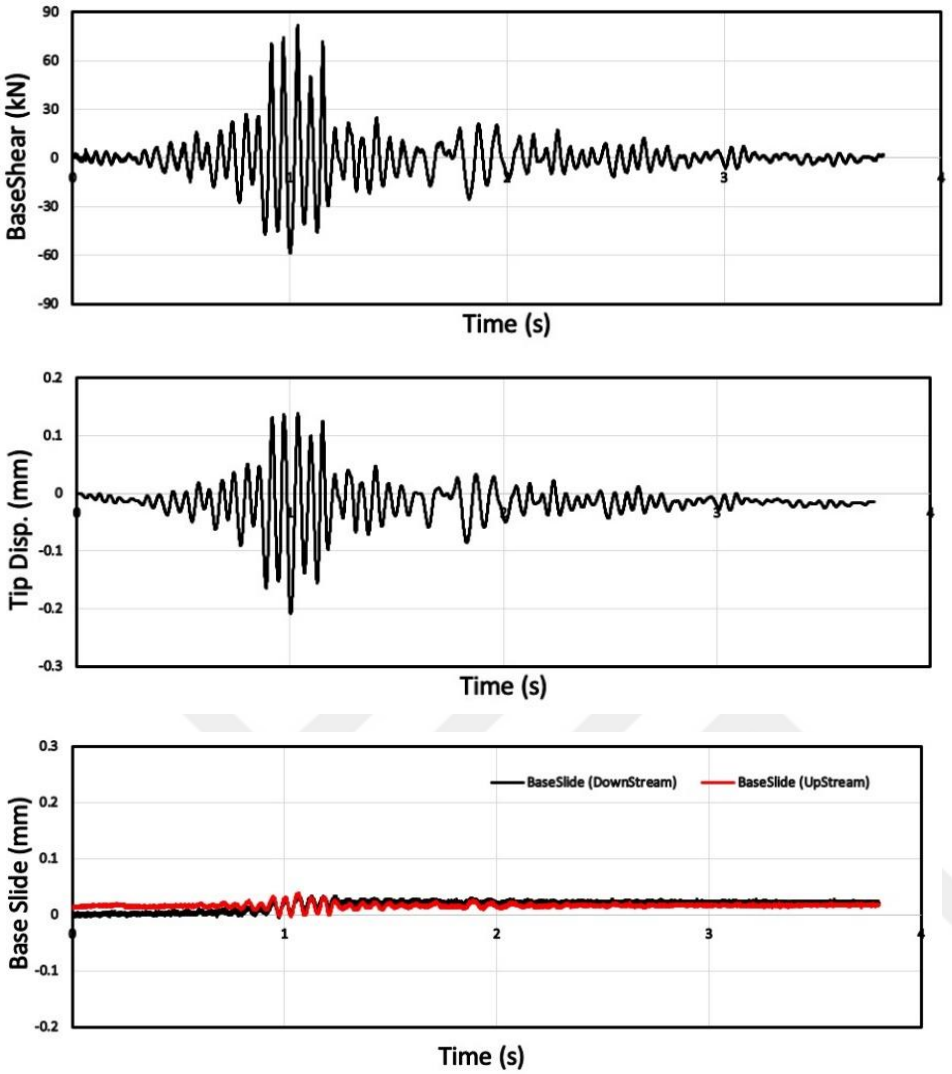

Figure 3-13 OBE recorded results

The axial force exhibited slight variations during the ground motion application. The axial load change versus time graph is shown in Figure 3-14. It can be observed that the maximum axial load variation was about 2% indicating an insignificant change. Moreover, the horizontal component of the pre-stressing force was calculated by using the horizontal component of the axial force. It was found that the pre-stressing effect during the OBE motion was around 0.1 kN as illustrated in Figure 3-14 showing that the axial force did not impose a significant lateral force on the system.

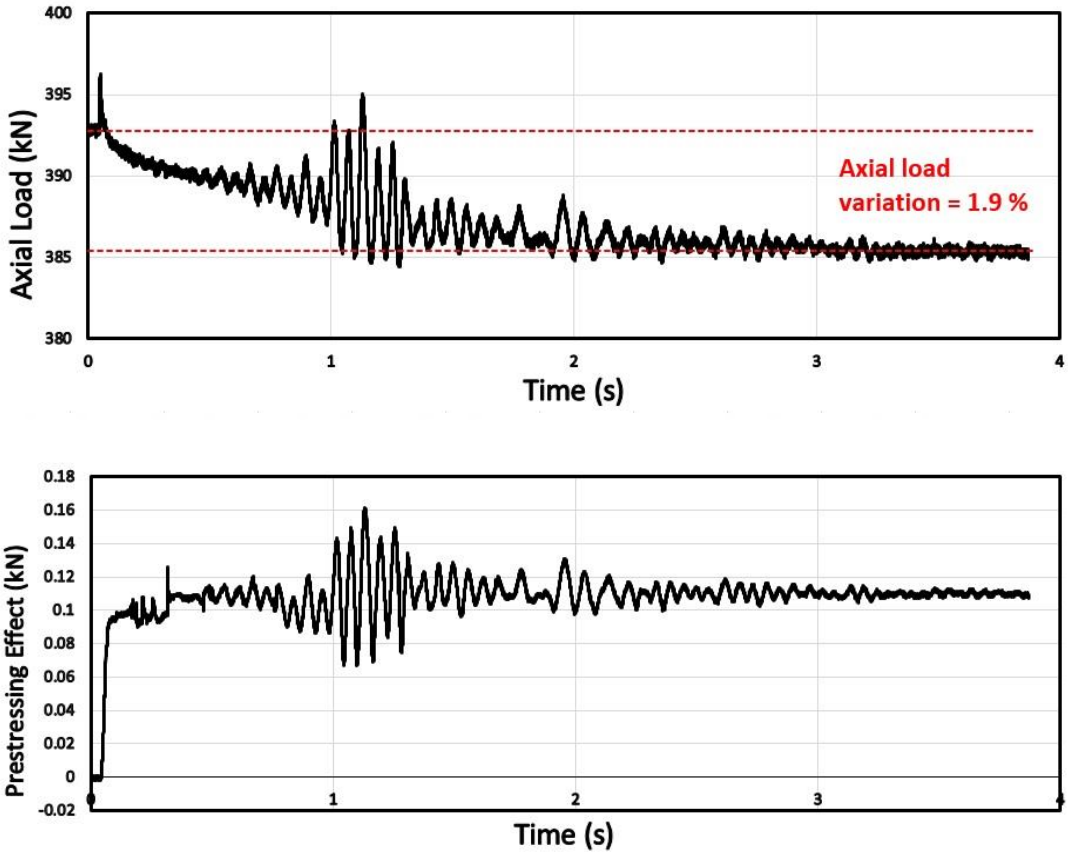

Figure 3-14 The axial load variation and the pre-stressing effect during the OBE motion

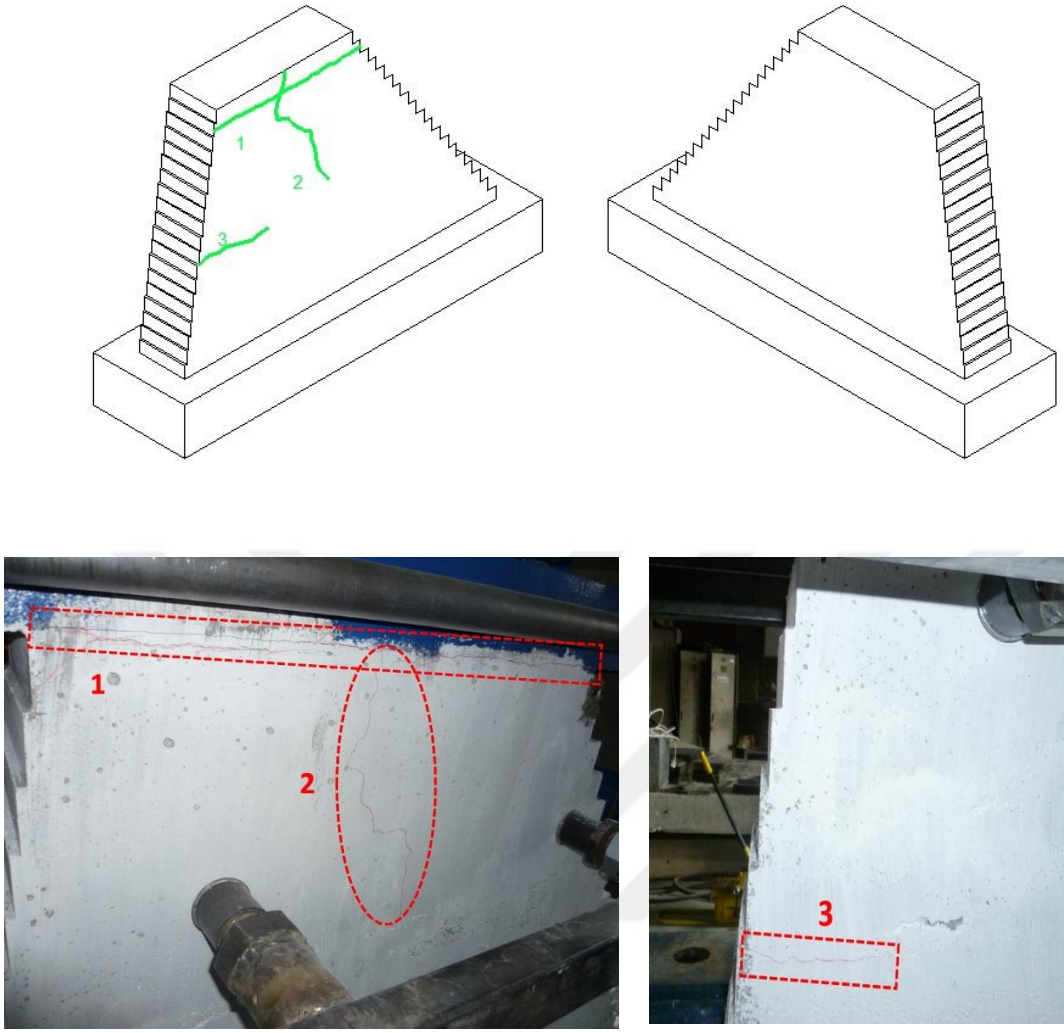

Figure 3-15 Crack Propagation (OBE)

3.5.2 MDE Experiment

Same dam specimen was subjected to the MDE motion with a peak acceleration of 0.15g and. Top displacements of around 0.2 and 0.4 mm appeared during the MDE ground motion in the upstream and downstream sides, respectively (Figure 3.16). A maximum sliding displacement of only 0.05 mm was observed during this test.

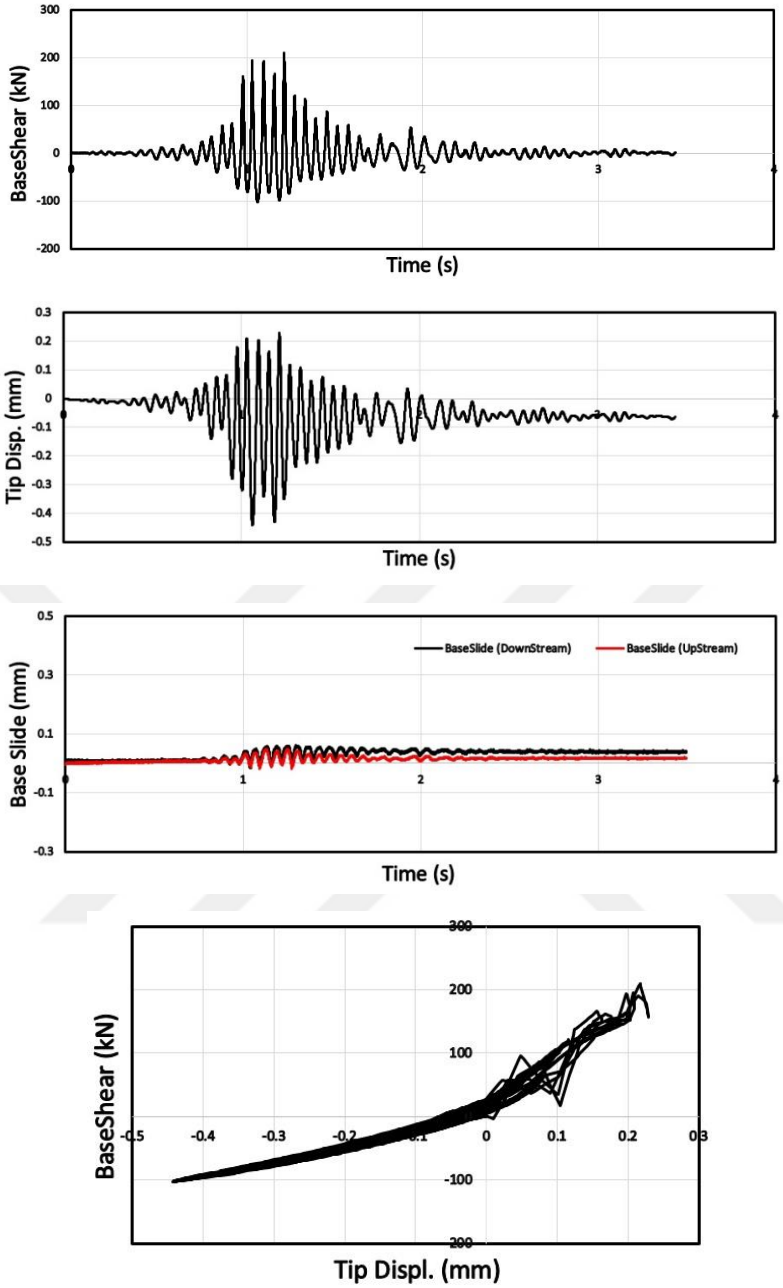

Figure 3-16 MDE recorded results

The axial force exhibited only slight variations during the MDE ground motion application. The axial load change versus time graph is shown in Figure 3-17. It can be observed that the maximum axial load variation was about 2% indicating an insignificant change. Moreover, the horizontal component of the pre-stressing force was calculated by using the horizontal component of the axial force. It was found that

the pre-stressing effect during the MDE motion was around 0.2 kN as illustrated in Figure 3-17 showing that the axial force did not impose a significant lateral force on the system similar to the OBE motion.

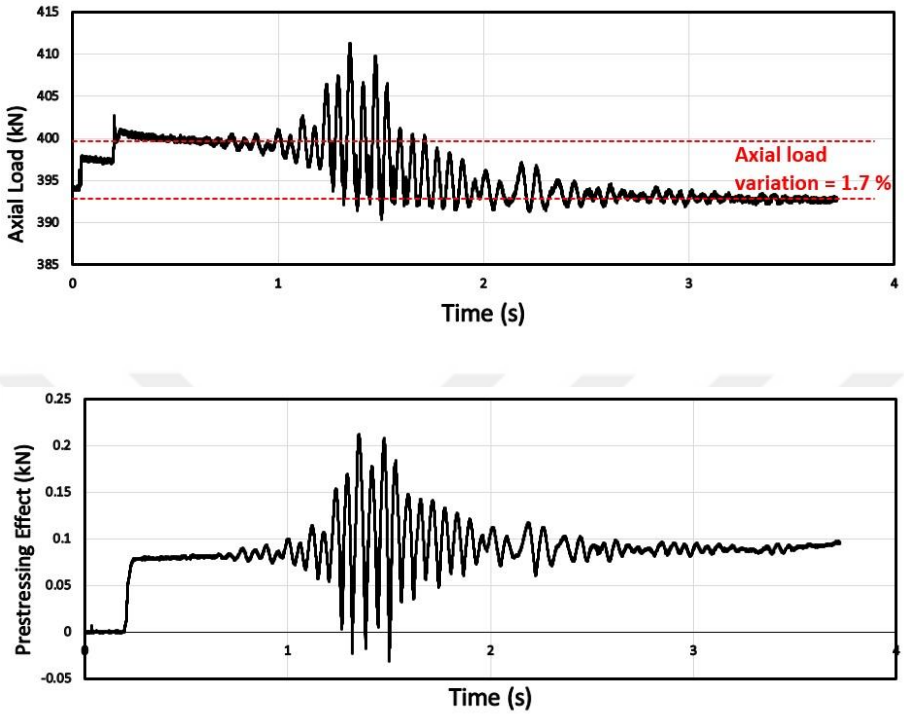

Figure 3-17 The axial load variation and the pre-stressing effect during the MDE motion

During the MDE ground motion, previous cracks remained unchanged. However, a horizontal crack at the CVC-RCC interface occurred at the upstream side of the monolith. It can be inferred that crack from the OBE motion further opened along the other face of the monolith (figure 3.18). It can be observed from the results that the MDE motion did not cause any significant further damage on the dam body.

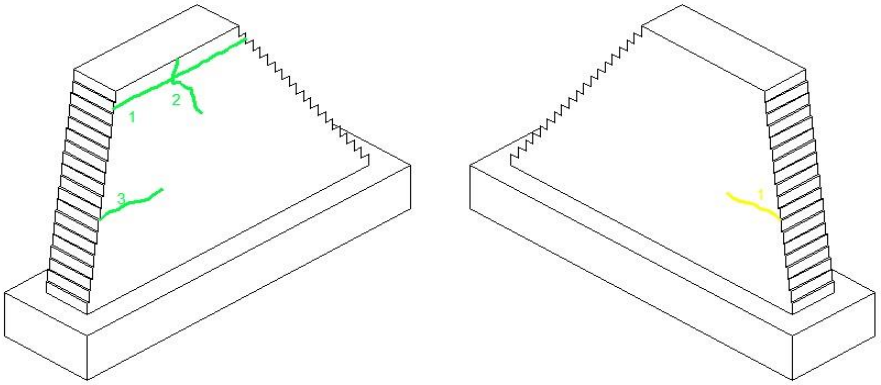

Figure 3-18 Crack propagation (MDE)

3.5.3 MCE Experiment

After the OBE and MDE motions, the specimen was subjected to the MCE ground motion with a peak acceleration of 0.33g. As it is visible from Figure 3.17, a residual base slide of around 1.2 mm occurred under the MCE motion. The reason behind this sliding was the weak bond between the dam body and the foundation arising from the smooth base situation. This slide was evident also from the tip displacement diagram where it showed the maximum tip displacement to be 2.23 mm. Upstream and downstream LVDTs exhibited a deviation of 0.19 mm which most probably stemmed from the rigid body rotation of dam specimen. Base slip occurred in two segment following each peak of the lateral load. It can be observed that the load-deflection response shown in Figure 3-17 exhibited a shift and residual displacement indicating the importance of the sliding.

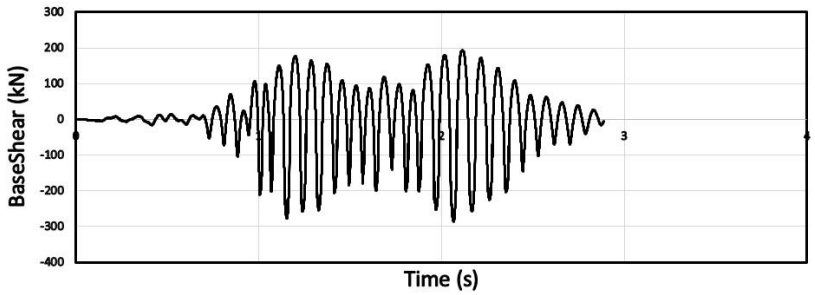

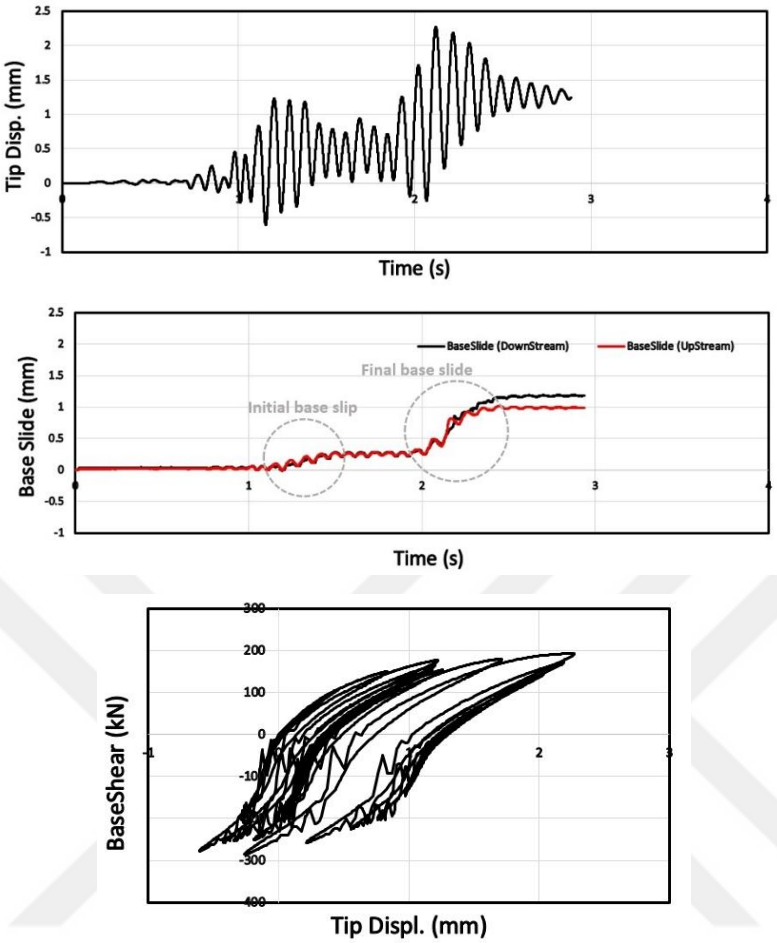

Figure 3-19 MCE recorded results

The axial force exhibited the highest variations during the MCE ground motion application. The axial load change versus time graph is shown in Figure 3-20. It can be observed that the maximum axial load variation was about 10%. This change can be seen acceptable based on engineering judgment. Moreover, the horizontal component of the pre-stressing force was calculated by using the horizontal component of the axial force. It was found that the pre-stressing effect during the MDE motion was around 0.8 kN as illustrated in Figure 3-20 showing that the axial force did not impose a significant lateral force on the system similar to the OBE and MDE motions.

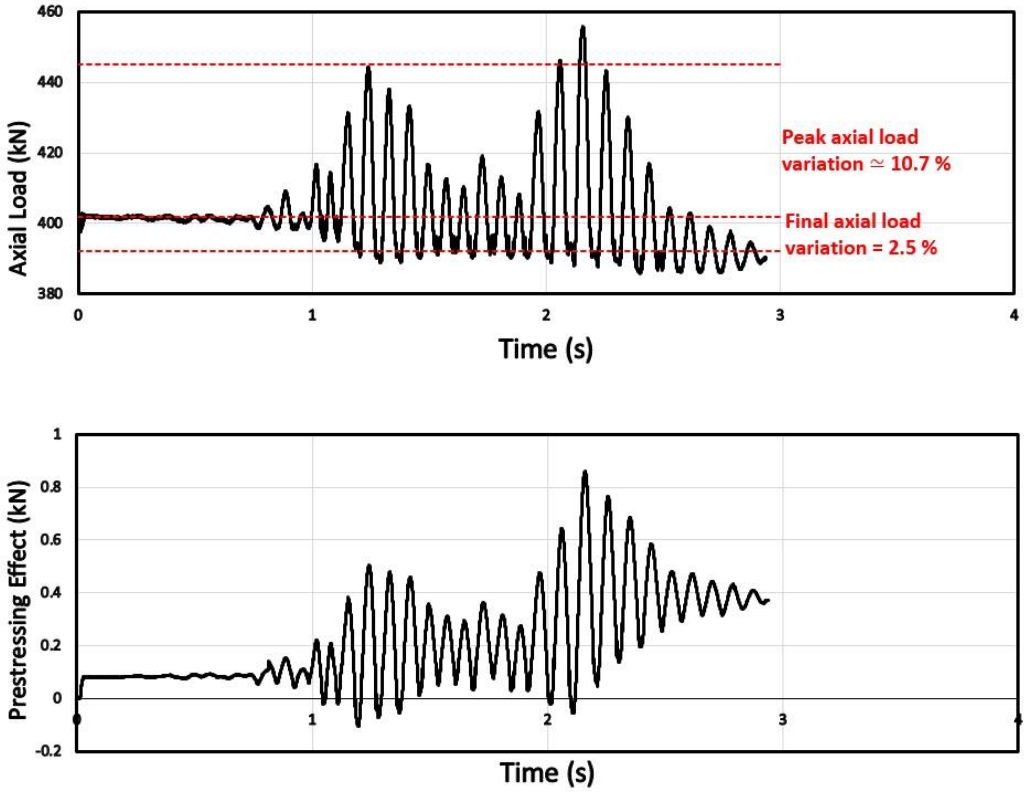

Figure 3-20 The axial load variation and the pre-stressing effect during the MCE motion

Crack patterns in both faces of the monolith expanded after the MCE ground motion as shown in Figure 3-18. OBE2, OBE3 and MDE1 cracks elongated to 12 cm, 21 cm and 11 cm, respectively. Furthermore, crack MDE1's width doubled to be 0.2 mm. A new crack also formed during the MCE motion with a width of 0.05 mm (Figure 3.21). The most important structural crack was observed at the dam-foundation interface. This crack caused the dam to slide and caused a residual slip of about 1.2 mm. It should be noted this slip value when multiplied with 75 (scale factor) would mean a final sliding of about 9 cm. Such a sliding amount is expected to break the water stoppers and cause significant damage.

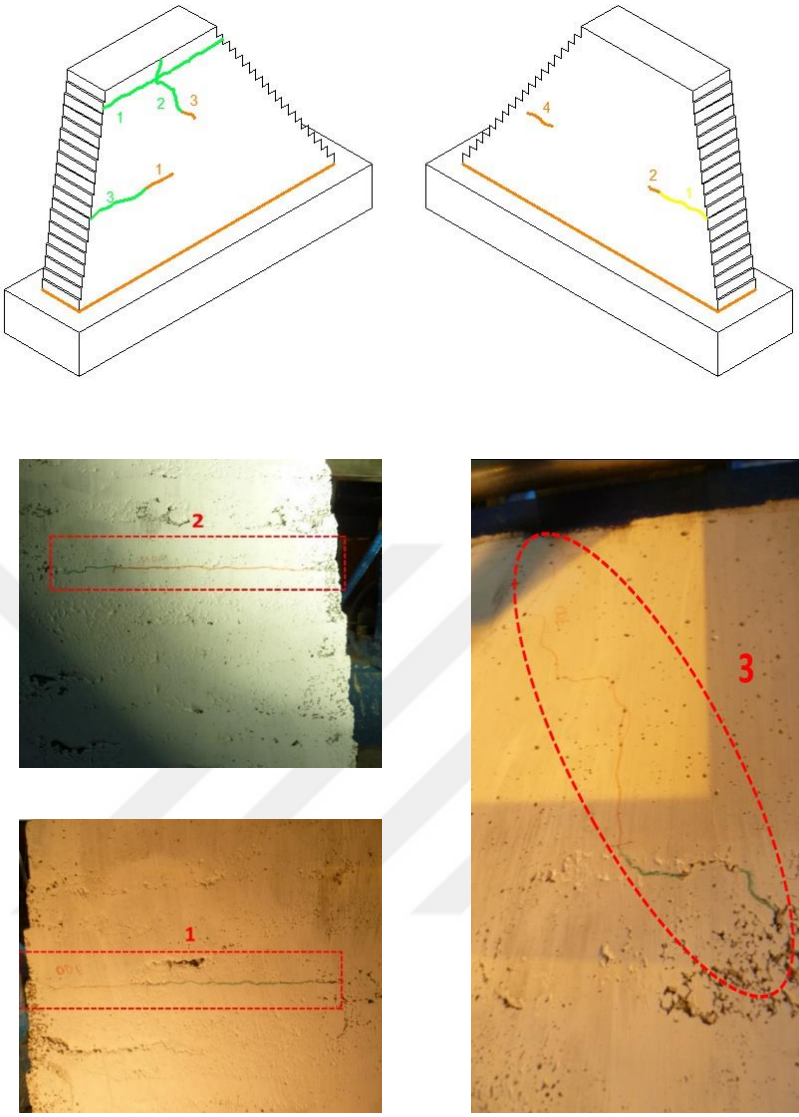

Figure 3-21 Crack propagation (MCE)

3.6 Sliding Analysis

The scaled dam monolith during MCE ground motion test was analyzed based on the method developed by Chopra et al. (1991b) in order to verify both credibility and accuracy of the method. The active forces during the seismic excitation consisted of hydrostatic (H_s), hydrodynamic (H_d), friction (F) and inertial forces. Dynamic

equilibrium equation in case of downstream sliding of dam during seismic excitation is given by (Chopra et al. 1991b):

$$M\ddot{s}(t) = -Ma(t) + H_s + H_d(t) - F \qquad \textbf{Equation 3-1}$$

where:

$$F = \mu(W - U) \qquad \textbf{Equation 3-2}$$

In the dynamic equilibrium equation s is the sliding displacement, M is the assigned numeric mass for the MCE scenario, W is the vertical force exerted by hydraulic pistons to mimic dam gravitational forces, U is the uplift forces which is zero in this context as a dry cold lift joint was assumed and μ is the friction coefficient between the dam body and foundation.

A MatLab program with was developed in the course of this study in order to solve the equations 3-1 and 3-2 by time integration to consequently determine the sliding displacements. A numeric mass (M_n) of 55 tons was used in the analysis in compliance with the test. The pre-stress vertical load was also considered by assigning a body mass (M) equal to 40 tons. In the case of acceleration in the upstream direction, the hydrodynamic and the dam body inertial forces were in downstream direction. Driving forces were the hydrostatic, hydrodynamic and inertial forces all of which were implemented directly from the experimentally recorded values. The program collects data from a file containing the time increments, the ground acceleration at that time increment and horizontal load applied to the specimen. Initially a critical acceleration, which is the minimum acceleration required to trigger the sliding, was calculated for given μ (Equation 3-3). In equation 3-3, the uplift force was zero and the M, M_n and H_s values were fixed for each time step.

$$a_c(t) = \frac{1}{M_n}(\mu(t) * (M - U) - H_s) \qquad \text{Equation 3-3}$$

The sliding acceleration ($\ddot{s}(t)$) was computed at time increments where the ground acceleration exceeded the calculated critical acceleration using equation 3-1. Then the base displacement was calculated by the numerical integration (Equation 3-4 and 3-5). The initial conditions, in other words, the base displacement and the base displacement velocity at time zero were set to be zero.

$$\dot{s}_{t+1} = \dot{s}_t + \frac{1}{2} * dt_{t+1} * (\ddot{s}_t + \ddot{s}_{t+1}) \qquad \text{Equation 3-4}$$

$$s_{t+1} = s_t + \frac{1}{2} * dt_{t+1} * (\dot{s}_t + \dot{s}_{t+1}) \qquad \text{Equation 3-5}$$

The results for the different friction coefficient values are shown in the Figure 3-22 for the μ values of 0.65, 0.68, 0.8 and 1. It should be noted that the friction coefficient of 0.68 was used as the friction coefficient of concrete-concrete cold joint of a small gravity dam model based on the study by Fronteddu et al. (1998). This value led to an ultimate sliding similar to the experiment, however, the sliding response during the ground motion did not match the experiment appropriately. It can be observed that the test data follows the friction coefficient of 0.8 until the end of 2nd sec and then makes a switch to the 0.68. This is an evidence of the fact that the friction coefficient varies with the increasing sliding displacements. The aggregate interlock was lost due to the movement at the joint level causing the reduction in friction coefficient value. Consequently, a variable friction coefficient was considered in the analysis. In the time period of 0-2.1 sec μ was taken as 0.8, while it was reduced 0.49 during 2.1-2.2 sec and further reduced to 0.47 after that time step. The friction coefficient values and their corresponding time periods were determined by trial and error procedure. Corresponding analysis resulted in a sliding history that is in reasonable agreement with the experiment. As shown in Figure 3.22, the dam body demonstrated sliding in two phases. The results of sliding analysis with different friction coefficients are shown in Figure 3-22. It can be observed that results are quite sensitive to the assumed coefficient of friction.

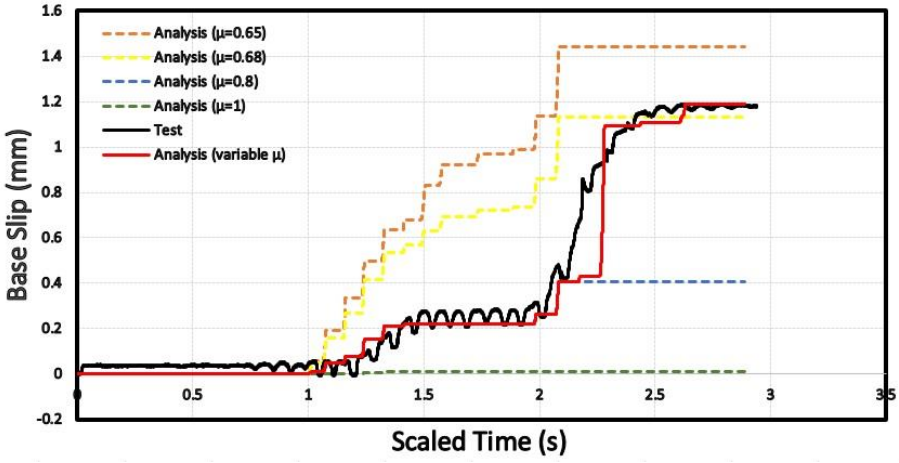

Figure 3-22 Base Slip comparison between Analysis and Test under MCE ground motion

The first product of the analysis according to Zhang and Chopra (1991b) was the base sliding acceleration at each time step as shown in equation 3-1 and discussed above. Adding the sliding acceleration contribution to the base acceleration, dynamic equation of the SDoF system was recalculated to compute the displacement of the SDoF model (Equation 3-6).

$$M\ddot{u}(t) + C\dot{u}(t) + Ku(t) = -M(a_{ground}(t) + \ddot{s}(t)) \qquad \text{Equation 3-6}$$

By assessing the system's dynamic behavior under the effect of ground acceleration and sliding acceleration simultaneously and computing equation 3-6 for u at each time step, the tip displacement can be computed as:

$$TopDisp_t = s_t + u_t \qquad \text{Equation 3-7}$$

By using a damping coefficient of 5% and fundamental period of T=0.105 sec for the SDoF model, the displacement history was computed as shown in Figure 3-23. It can be observed that the SDoF model was capable of matching the wave form of the recorded displacements. However, it slightly overestimated the peak values possibly due to change of instantaneous damping which was not included in the analysis.

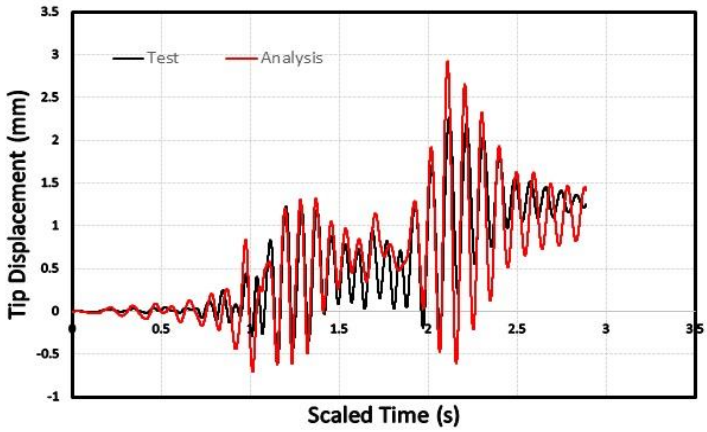

Figure 3-23 Tip Displacement comparison between Analysis and Test under MCE ground motion

3.7 Pushover Experiment

A pushover test was conducted on the same dam monolith to obtain the extreme capacity of the system. Scaled dam monolith under 400 kN of vertical load was exposed to gradually increasing lateral load from zero until the specimen's failure. The sample was unloaded prior to reaching it's capacity and reloaded again to observe the dam behavior during unloading. The results are shown in Figure 3-21 and 3-22. It can be observed that the scaled dam monolith demonstrated considerable elastic deformation during first cycle with peak of up to around 282 kN while the second cycle triggered complete failure that is in the form of base sliding. It is worth mentioning that all the cracks in pushover test occurred under lateral load above 294 kN. The scaled dam behavior during pushover test is presented in Figure 3.21.

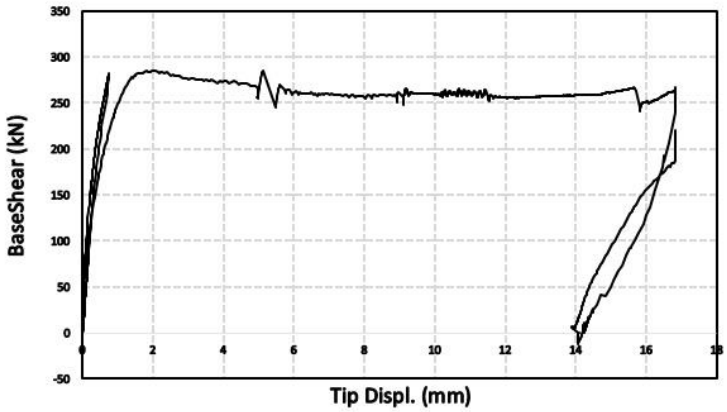

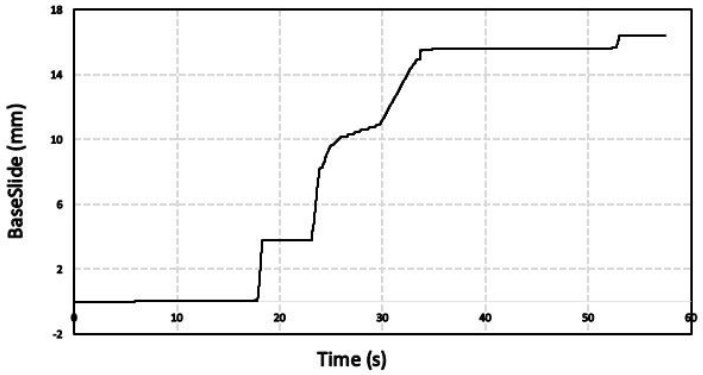

Figure 3-24 Pushover recorded results

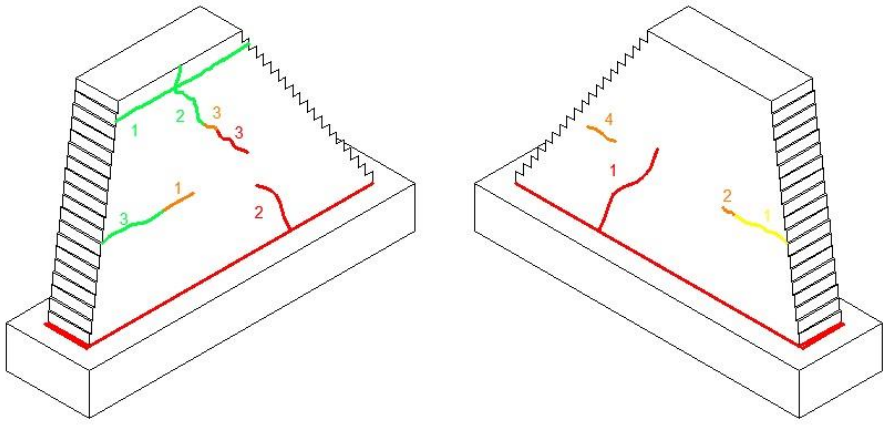

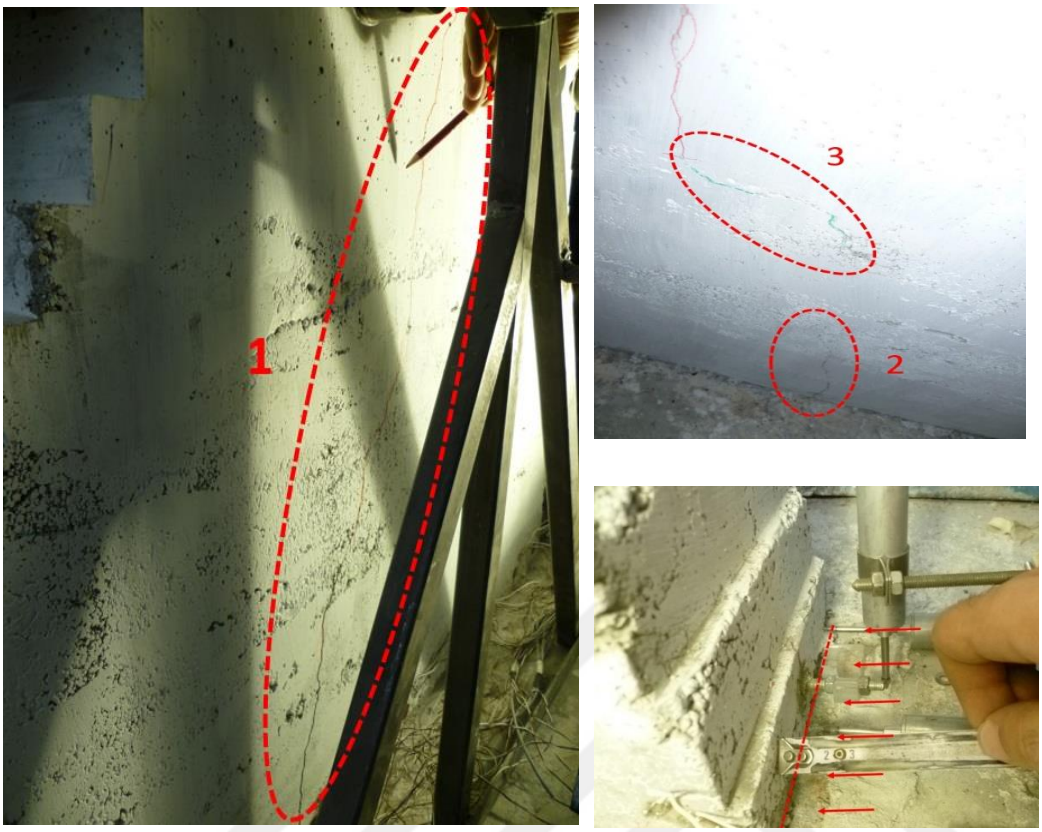

Figure 3-25 Crack propagation (Pushover)

Crack distribution after the pushover test is shown in Figure 3-22. Overturning moment initiated vertical cracks at both sides of dam monolith. Cracks P1 and P2 with a width of 1.75 mm and length of 184 cm and 54 cm formed on the specimen. The cracks showed that the dam monolith exhibited a combined rigid body sliding and body damage during the pushover test. The previously initiated vertical crack (OBE2 continued by MCE3) was extended by 36 cm widening to 0.2 mm. However the performance was still dictated by the base crack extending from the upstream to downstream side. As a result, it can be mentioned that the specimen failed due to sliding at base (Figure 3.22).

3.8 Identification of dynamic properties of the specimen

Dynamic properties of the dam specimen including, the natural period and the equivalent viscous damping, for three ground motions were acquired using the collected data. According to method proposed by Molina et al. (1999), the equation of motion is driven at discrete time series:

$$m\,a(n) + r(n) = f(n) \qquad \text{Equation 3-8}$$

In equation above, m is the mass matrix, a(n), f(n) and r(n) are the acceleration, external force and restoring force at specific time interval respectively. In a dynamic system modeled by equivalent viscous damping, the restoring force at any time segment can be defined as:

$$[u^T(n) \quad v^T(n) \quad 1] \cdot \begin{bmatrix} k^T \\ c^T \\ o^T \end{bmatrix} = r^T(n) \qquad \text{Equation 3-9}$$

where k is secant stiffness and c is damping matrices. u and v are the displacement and velocities at the corresponding degrees of freedom and o is an equilibrium constant.

Equation 3.8 is solvable benefitting from collected test data at N time intervals as long as N is 1 unit greater than two times of degrees of freedom number. By choosing a time window containing steps more than or equal to N, least square solution is obtained for k and c. As presented by Maia and Silva (1997), frequency and damping coefficient can be extracted as follows:

$$s\begin{bmatrix} C & M \\ M & 0 \end{bmatrix} v + \begin{bmatrix} K & 0 \\ 0 & -M \end{bmatrix} v = 0 \qquad \text{Equation 3-10}$$

$$s_1, s_1^* = w_1\left(\zeta_1 \pm i\sqrt{1-\zeta_1^2}\right) \quad where \quad i^2 = -1 \qquad \text{Equation 3-11}$$

In equation 3.11, $w_1\ and\ \zeta_1$ are natural frequency and equivalent viscous ratio at first mode. A window of 1000 data points with 20 data point increments were used. The

data for first 0.5 sec is eliminated since there was no major displacement at that time period. Secant stiffness matrix was used for fundamental period calculation as this approach results in better correlation with observed damage. The hydrostatic force and corresponding displacement were ignored during the calculations (Aldemir, 2016). Fundamental period of undamaged dam monolith was determined to be 0.06 sec, and remains nearly constant throughout OBE and MDE experiments while this value extends to 0.085 sec. Fundamental period change during MCE was due to the base slide and the extended-cracking propagated along this test besides the previous cracking (Figure 3.23).

Identified material damping time history is presented in figure 3.26. Provided red line in the graph represents USACE (2003) recommended values for damping which is 5% for OBE and MDE ground motions and 7% for MCE. In case of two preceding ground motions, identified damping matches the recommended value. On the other hand, in the latter one, the recommended value from USACE (2003) remained above the identified damping history. It is important to mention that damping values represented in here corresponds to the material damping of a single monolith excluding interactions between dam monoliths.

In addition to identification of dynamic properties of the dam specimen, the damping ratio for the cycles containing the highest shear demand was determined for each earthquake level by using the proposed method by Megally (1998) (Equation 3.12). Principals of this method is presented in Figure 3.27. The damping for the OBE, MDE and MCE ground motions turned out to be 2%, 1% and 9%, respectively. The damping value for OBE and MDE motions did not appropriately match the values obtained from identification however, the method proposed by Megally (1998) led to the similar damping that the identifications presented.

$$\xi = \frac{1}{4\pi} * \frac{Dissipated\ Energy\ in\ Cycle}{Elastic\ Energy} \qquad \text{Equation 3-12}$$

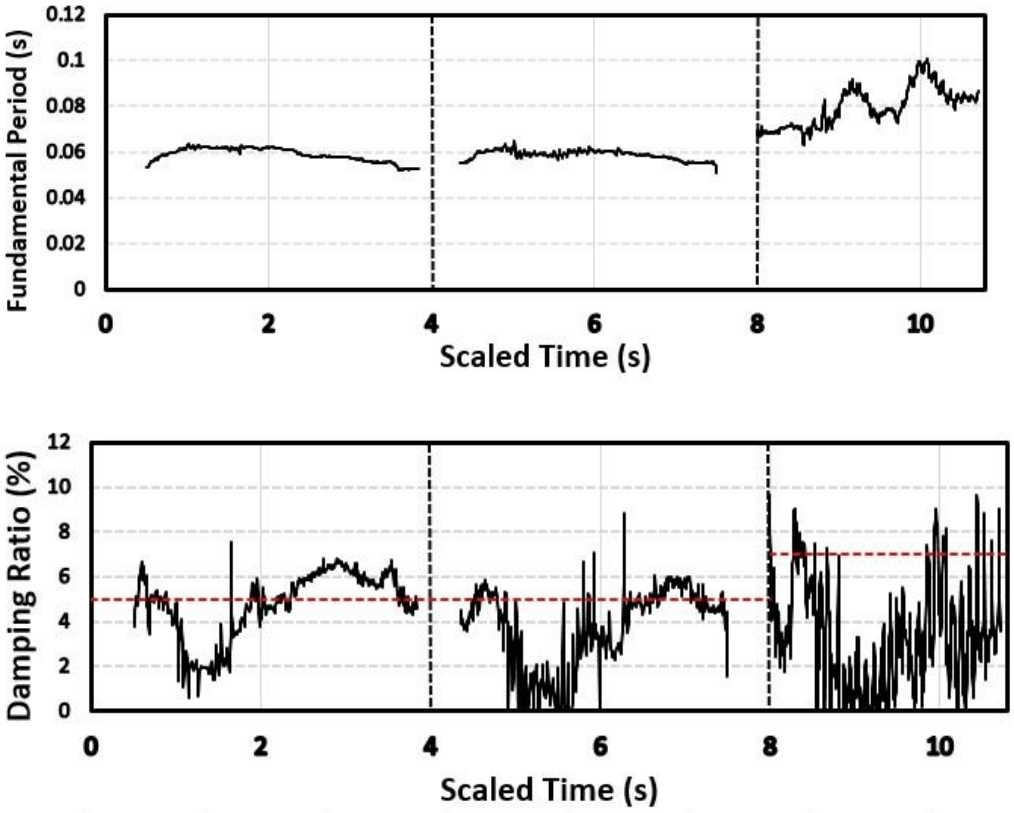

Figure 3-26 Scaled dam monolith dynamic properties; Top: Fundamental period variation, Bottom: Damping ratio variation

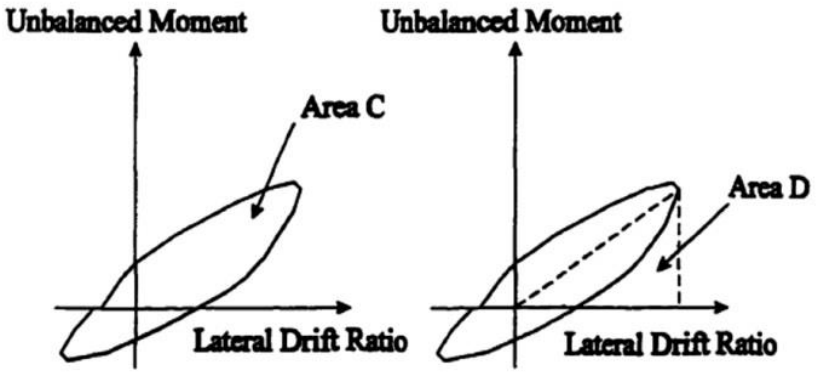

Figure 3-27 Hysteretic damping plot from Megally (1998)

3.9 Strain Gauges

Along the dam base 8 strain rosettes were attached. These strain rosettes were used to measure strains in the three direction allowing users to draw maximum principal stress, minimum principal stress and orientation angle from recorded data. Unfortunately, the rosette number 5 was out of order; consequently, the computations were completed using data from the rest of rosettes. The first and second principal stresses for all of ground motions are illustrated in Figure 3.28. Referring to the first principal strain diagram, strain recorded by rosette number 7 exceeded the cracking strain of concrete during MCE ground motion. Principal strain orientation for mentioned rosette is 44.9° (counterclockwise) and this matched with crack pattern MCE1 and MCE2 as it is visible in Figure 3.21. The key cracking observation at the dam base during MCE motion was confirmed with the measured strains.

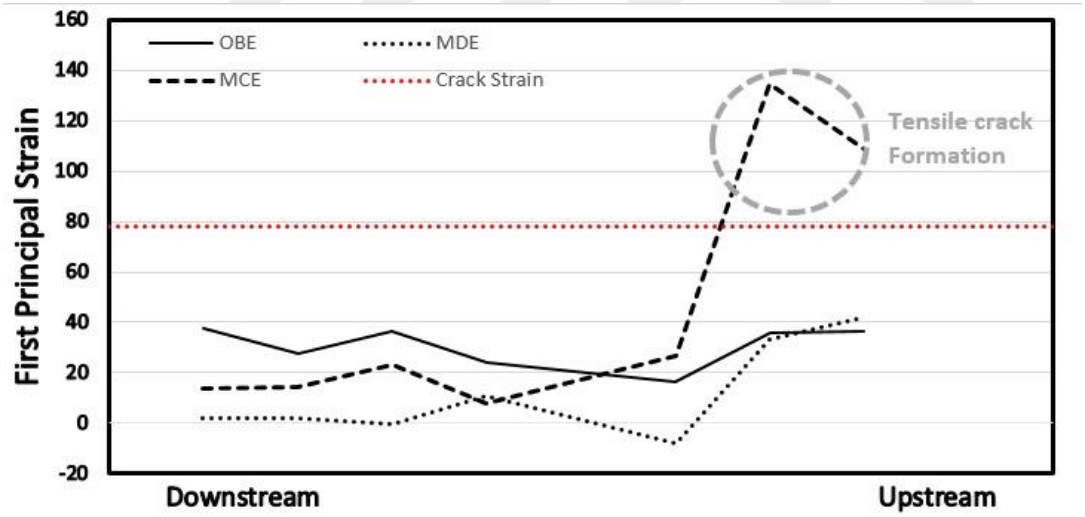

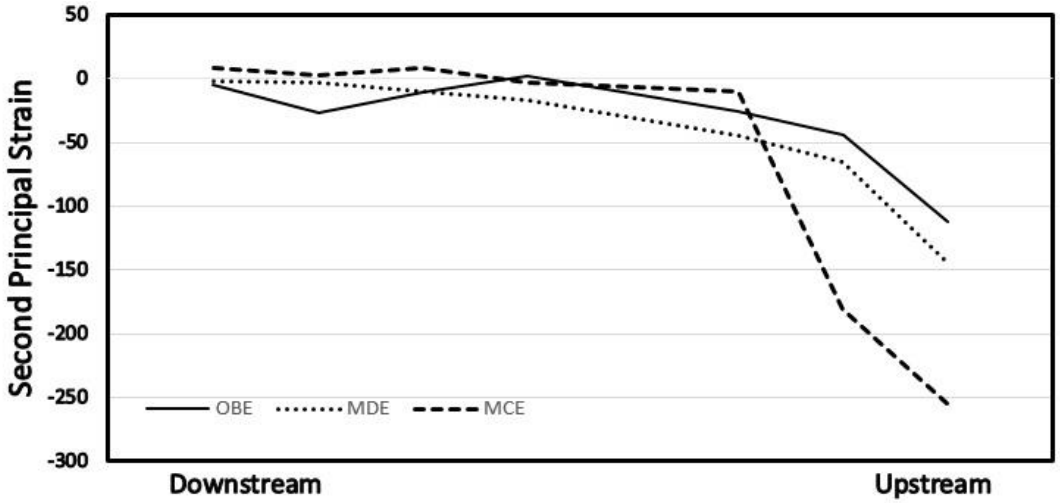

Figure 3-28 Principal Strain distributions along the dam base

3.10 Comparisons with a Companion Specimen

In a companion study, Aldemir et al. (2015) carried out a similar SDoF pseudo-dynamic test for a scaled dam constructed on an intentionally roughened foundation with 6 mm indentation. In that study, it was reported that the scaled dam monolith failed due to the excessive crack propagation within dam body as shown in Figure 3-30. Base displacement time histories for smooth base (SB) and roughened base (RB) during MCE test results demonstrate that a slip of 1.2 mm was observed in the SB specimen whereas 0.1 mm interface displacement occurred in the RB specimen (Figure 3-29). As it is visible from Figure 3-30 severe cracks appeared in the RB specimen body while SB specimen suffered cracking throughout the dam-foundation interface during the pushover test.

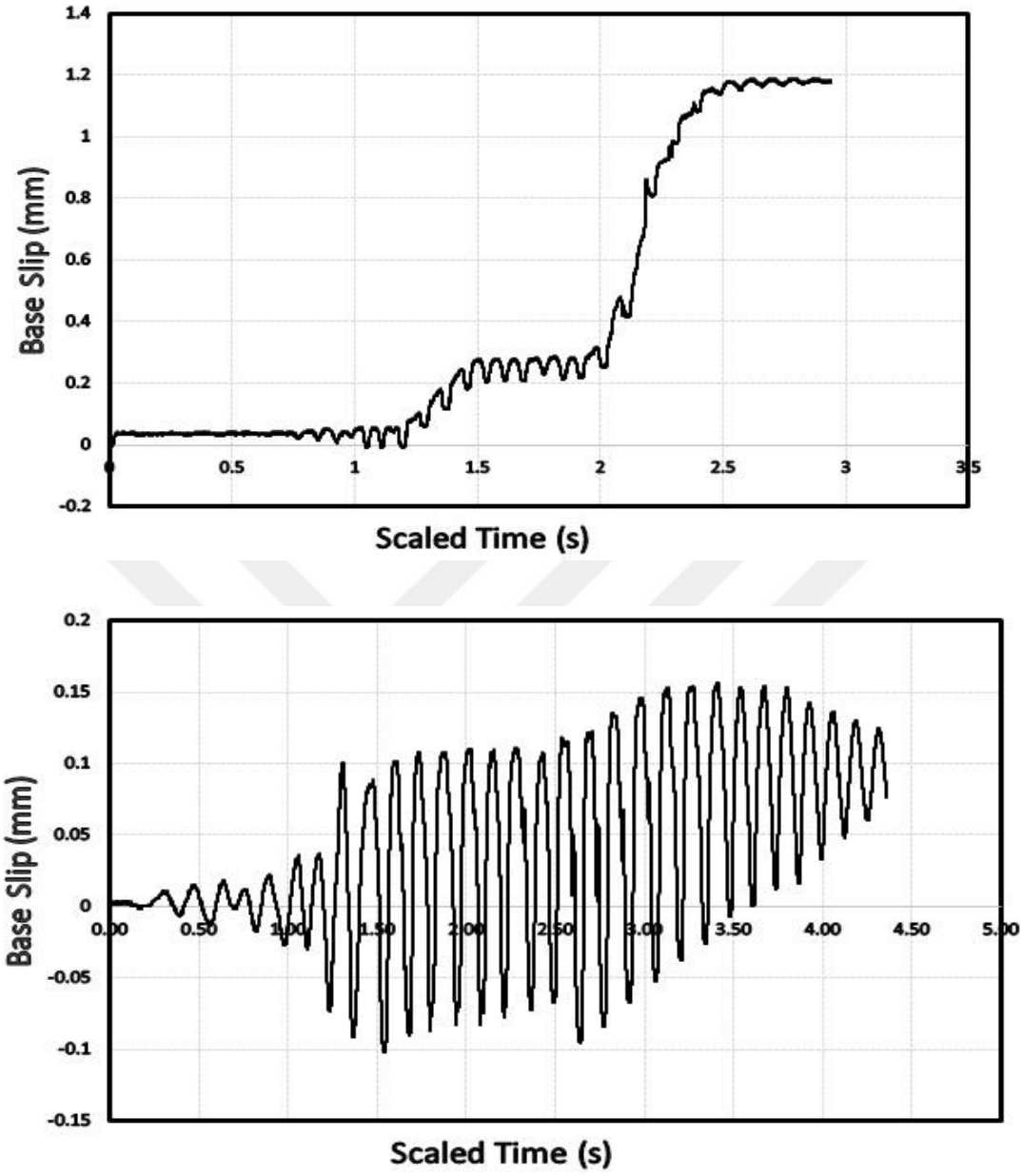

Figure 3-29 Base displacement records for SB and RB specimens during MCE ground motion (Aldemir, 2015)

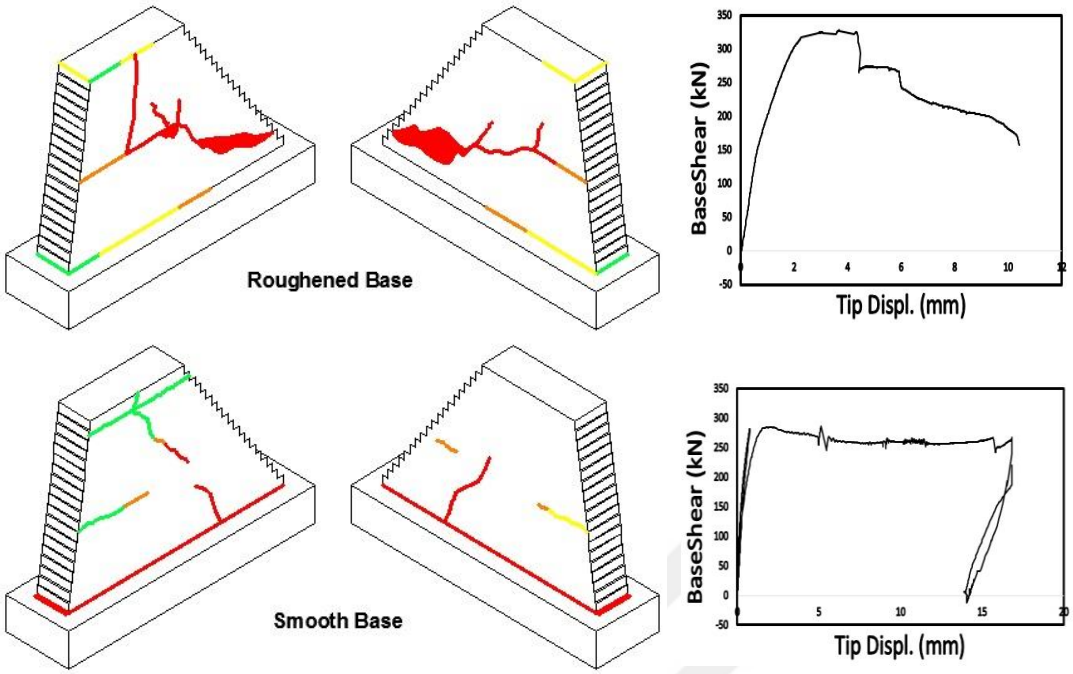

Figure 3-30 Crack propagation during Pushover test (Aldemir, 2015)

The comparison between the two specimens shows that upon possibility of having slip deformation, the cracking on the body reduced. It should be noted, that both slip and inclined body cracking are unacceptable for satisfactory dam performance. However, knowing the type of failure mode in an extreme event is crucial in the design process in order to take the necessary measures (e.g. design of water stoppers or dam upstream and downstream slopes.)

CHAPTER 4

CONCLUSIONS

4.1 Summary of Results

The scaled concrete gravity dam specimen tested in the scope of this study was constructed on a smooth dam foundation interface with a cold joint. The weak bond between the monolith and foundation resulted in base slip towards the downstream direction during the MCE earthquake and the pushover test. Test results were compared with the analytical results obtained by the numerical procedure of Chopra and Zhang (1991b) proposed for the analysis of the sliding of dams. A good agreement was observed between the test results and the numerical simulation upon the proper choice of the coefficient friction. A comparison was then made with the results of Aldemir et al. (2015) who tested a similar specimen but with a roughened dam-foundation interface. In that test, the failure mode was severe body cracking with negligible base slide. This points out the importance of dam-foundation interface conditions in defining the final expected damage state during an earthquake.

4.2 Conclusions

Conclusions drawn based on the test results are given below:

1- The scaled dam model of Melen RCC Dam if built with a smooth dam-foundation interface (key height of 0.1 mm in the test corresponding to 7.5 mm in the prototype dam) is expected to sustain no significant damage during OBE and MDE motion. However, these base conditions resulted in significant base sliding (about 1.2 mm in the scaled test and 90 mm in the prototype dam). Such magnitudes of base sliding of has to be limited as the excessive base

displacement would cause damages in the water-stoppers which may lead to water leakage, undesired uplift forces at the dam base, and the occurrence of permanent displacements that are impractical to fix.

2- The sliding analysis of the Chopra and Zhang (1991b) was found to be in reasonable agreement with the test results. This provides confidence for its use in the case of sliding.

3- A companion specimen by Aldemir (2015) with a rough dam-foundation interface (key height of 6 mm in the test corresponding to 450 mm in the prototype dam) did not exhibit any significant sliding displacements. This comparison shows that dam sufficient base roughness (key height) is crucial to eliminate sliding induced damage during the design of concrete gravity dams. As suggested by FERC (2016) dam foundation interface of the gravity dams must be keyed and special attention should be given to its construction.

Further studies are recommended to observe the combined sliding and the dam body damage situations by using experimental and computational techniques in the future.

REFERENCES

Chopra, A.K., Chakhrabarti, P., Gupta, S. (1980). *Earthquake response of concrete gravity dams including hydrodynamic and foundation interaction effects*. University of California, UCB/EERC-80/01.

Takanashi, K. (1982). *Pseudo-dynamic response by computer-actuator hybrid system and it's application to aseismic design of steel structures*. Springer-Verlag Berlin Heidelberg.

Fenves, G., Chopra, A.K. (1984). *EAGD-84 a computer program for earthquake analysis of concrete gravity dams*. University of California, UCB/EERC-84/11.

Mahin, S.A., Shing, P.S. (1985). *Pseudodynamic method for seismic testing*. Journal of Structural Engineering, 111(7).

Fenves, G., Chopra, A.K. (1985). *Simplified analysis for earthquake resistant design of concrete gravity dams*. University of California, UCB/EERC-85/10.

Durin, Z.H. (1987). *Experimental and finite element studies of a large arch dam.* California Institute of Technology, EERL 87-02.

Donlon, W.P. (1989). *Experimental investigation of the nonlinear seismic response of concrete gravity dams*. California Institute of Technology, EERL 89-01.

Chopra, A.k.,Zhang, L. (1991a). *Earthquake –induced base sliding of concrete gravity dams*. Journal of Structural Engineering Vol. 117, No12.

Chopra, A.k.,Zhang, L. (1991b). *Base sliding response of concrete gravity dams to earthquakes*. University of California at Berkeley, UCB/EERC-91/05.

Nakashima, M., Kato, H., Takaoka, E. (1992). *Development of real-time pseudo dynamic testing.* Earthquake Engineering and Structural Dynamics.

Hui, P.K. (1992). *Dynamic behavior of base cracked gravity dam by the way of the hybrid frequency time domain procedure*. University of British Columbia.

Danay, A., Adeghe, N. (1993). *Seismic-induced slip of concrete gravity dams*. Journal of Structural Engineering, 1562.

Bhattacharjee, S.S., Leger, P. (1994). *Application of NLFM models to predict cracking in concrete gravity dams*. Journal of Structural Engineering, 4766.

Proulx, J., Paultre, P. (1996). *Experimental and numerical investigation of dam-reservoir-foundation interaction for a large gravity dam*. Canadian Journal of Civil Engineering, 24:90-105.

Mir, R.A., Taylor, C.A. (1996). *An investigation into the base sliding response of rigid concrete gravity dams dynamic loading*. Earthquake Engineering and Structural Dynamics, 7998.

Ghobarah, A., Ghaemian, M. (1998). *Experimental study of small scale dam models*. Journal of Engineering Mechanics, 16195.

Fronteddu, L., Leger, P., Tinawi, R. (1998). *Static and dynamic behavior of concrete lift joint interfaces*. Journal of Earthquake Engineering, 15857.

Molina, F.J., Pegon, P., Verzeletti, G. (1999). *Time-domain identification from seismic pseudo dynamic test results on civil engineering specimens*. International Conference on Identification in Engineering Systems, 29–31.

Tinawi, R., Leger, P., Lecrec, M., Cipolla, G. (2000). *Seismic safety of gravity dams: from shake table experiments to numerical analyses*. Journal of Structural Engineering, 20153.

Chuhan, Z., Guanglun, W., Shaomin, W., Yuexing, D. (2002). *Experimental tests of rolled compacted concrete and nonlinear fracture analysis of rolled compacted concrete dams*. Journal of Materials in Civil Engineering.

Morin, P., Leger, P., Tinawi, R. (2002). *Seismic behavior of post-tensioned gravity dams: shake table experiments and numerical simulations*. Journal of Structural Engineering.

Ghanaat, Y. (2004). *Failure modes approach to safety evaluation of dams*. World Conferences on Earthquake Engineering, 1115.

Uchita, Y., Shimpo, T., Saouma, V. (2005). *Dynamic centrifuge tests of concrete dam*. Earthquake Engineering and Structural Dynamics. 34:1467-1487.

Ghanaat, Y., Ramussen, B. (2005). *Evaluation of seismic stability of Claytor dam using linear and nonlinear time history analyses*. United State Society on Dams.

US Army Corps of Engineers. (2006). *Roller-Compacted Concrete*. EM1110-2-2006.

Wang, H., Li, D. (2006). *Experimental study of seismic overloading of large arch dam*. Earthquake Engineering and Structural Dynamics, 199-216.

Rochon-Cyr, M., Leger, P. (2009). *Shake table sliding response of a gravity dam model including water uplift pressure*. Engineering Structures 1625-1633.

Akkar, S. (2010). *Probabilistic seismic risk analysis of Melen dam for design spectrum calculations*. Report No: 2010-03-03-1-01-04, METU (in Turkish).

Basili, M., Nuti, C. (2011). *A simplified procedure for base sliding of concrete gravity dams under seismic action*. ISRN Civil Engineering, 4130357.

Chen, J., Wang, M., Fan, S. (2012). *Experimental investigation of small-scaled model for powerhouse dam section on shaking table*. Structural Control and Health Monitoring, 10.1002/stc.1489.

Kurt, E.G., Kurc, O., Binici, B., Ozcebe, G. (2012). *Performance examination of two seismic strengthening procedures by pseudodynamic testing*. Journal of Structural Engineering, 138(1):31-41.

Yucel, A.R. (2013). *Seismic analysis of concrete gravity dams including dam-foundation-reservoir interaction*. Middle East Technical University.

Aldemir, A., Binici, B., Arici, Y., Kurc, O., Canbay, E. (2015). *Pseudo-dynamic testing of a concrete gravity dam*. Earthquake Engineering and Structural Dynamic.

Aldemir, A. (2016). *Seismic performance evaluation of roller compacted concrete gravity dams by using pseudo-dynamic test method*. Middle East Technical University.

Binici, B., Aldemir, A., Gharibdoust, A. (2016). *Effect of base roughness on seismic response of concrete gravity dams*. International Committee on Large Dams.

Federal Energy Regulatory Commission, (2016). Engineering guidelines for evaluation of hydropower projects. http://www.ferc.gov/industries/hydropower/safety/guidelines/eng-guide/chap3.asp

APPENDIX A

PROGRAM DEVELOPED FOR SLIDING ANALYSIS PROPOSED BY CHOPRA et al. (1991b)

```
clc
clear all
%% Required Data
rho=1; % water density
mud=1; % Coeff. of friction (dynamic)
h=0.95; % water height (m)
hd=0.95; % dam height (m)
U=0; % Uplift force
Hs=17000; % Hydrostatic force (kg)
M=40000; % Mass of dam (kg)
Mn=55000; %Numeric Mass of dam (kg)
g=9.81;

%% Initiation
data=xlsread('Book11.xlsx'); % Read ground acceleration and
corresponding forces
t(:,1)=data(:,1);
ag(:,1)=data(:,2); % Ground acceleration
fh(:,1)=data(:,3); % Horizontal forces

fh(:,1)=fh(:,1)*1000/g;
fh=ones(size(fh,1),1)*Hs+fh;

%% Variable Coefficient of Friction
for ii=1:length(data)
    if t(ii,1)<=2.1
        mus(ii,1)=0.8;
    elseif 2.1<t(ii,1)&&t(ii,1)<=2.2
        mus(ii,1)=0.49;
    else
        mus(ii,1)=0.465;
    end
    ac(ii,1)=1/Mn*(mus(ii,1)*(M)-Hs); % ac is critical acceleration
in g units
end
```

```
%% Acquiring sliding

% for k=1:length(data)
%     if ag(k,1)>=ac
%         value(k,1)=ag(k,1)-ac;
%     else
%         value(k,1)=0;
%     end
% end
for i=1:length(data)

        if ag(i,1)>=ac(i,1)
            dds(i,1)=1/Mn*g*fh(i,1)-1/Mn*(mus(i,1).*(M*g-U*g)); %
Acquiring sliding acceleration
            if dds(i,1)<=0
                dds(i,1)=0;
            end
        else
            dds(i,1)=0;
        end
end
disp(1,1)=0; vel(1,1)=0;
for j=2:length(data)
    dt(j,1)=t(j,1)-t(j-1,1);
    if dds(j,1)==0
        vel(j,1)=0;
    else
        vel(j,1)=vel(j-1)+dt(j,1)*1/2*(dds(j-1,1)+dds(j,1));
    end
    disp(j,1)=disp(j-1)+dt(j,1)*1/2*(vel(j-1,1)+vel(j,1));

end

%% Top Displacement (SDoF)(Central Difference Method)
% Initial Conditions
u(1,1)=0; u(2,1)=0;
damp=0.05; % damping percantage from MCE identification
Period=0.105;
c=2*Mn*damp*(2*pi/Period);
kk=(2*pi)^2*Mn/Period^2; % Period is 0.08 from MCE identification

for i=2:(length(data)-1)
    kcap(i,1)=Mn/dt(i,1)^2+c/2/dt(i,1);
    a(i,1)=Mn/dt(i,1)^2-c/2/dt(i,1);
    a1(i,1)=a(i,1).*u(i-1,1);
    b(i,1)=kk-2*Mn/dt(i,1)^2;
    b1(i,1)=b(i,1).*u(i,1);
    p(i,1)=Mn*(ag(i,1)+dds(i,1));
    pcap(i,1)=p(i,1)-a1(i,1)-b1(i,1);
    u(i+1,1)=pcap(i,1)/kcap(i,1);
end
for ali=1:length(data)
    TopDisp(ali,1)=disp(ali,1)+u(ali,1);
```

```
end

%% Outputs
plot(t(:,1),disp(:,1))
xlabel('t')
ylabel('slide')
```